Pergamon

Geochimica et Cosmochimica Acta, Vol. 66, No. 5, pp. 881–901, 2002

0016-7037/02 $22.00 + .00

PII S0016-7037(02)00807-9

Rare gas isotopes and parent trace elements in ultrabasic-alkaline-carbonatite complexes, Kola Peninsula: Identification of lower mantle plume component

I. N. TOLSTIKHIN,[1,*] I. L. KAMENSKY,[1] B. MARTY,[2] V. A. NIVIN,[1] V. R. VETRIN,[1] E. G. BALAGANSKAYA,[1] S. V. IKORSKY,[1] M. A. GANNIBAL,[1] D. WEISS,[3] A. VERHULST,[3] and D. DEMAIFFE[3]

[1]Geological Institute, Kola Scientific Centre, Russian Academy of Sciences, Apatity 184200, Russia
[2]Centre National de la Recherche Scientifique, Centre de Recherches Pétrographiques et Géochimiques (C.R.P.G.), B.P. 20, 54501 Vandoeuvre-lès-Nancy Cedex, France
[3]Pétrologie et Géodynamique Chimique, Département des Sciences de la Terre et de l'Environnement, Faculté des Sciences, Université Libre de Bruxelles, Avenue F.D.Roosevelt 50 B-1050 Bruxelles, Belgique

(*Received April* 17, 2000; *accepted in revised form June* 11, 2001)

Abstract—During the Devonian magmatism (370 Ma ago) ~20 ultrabasic-alkaline-carbonatite complexes (UACC) were formed in the Kola Peninsula (north-east of the Baltic Shield). In order to understand mantle and crust sources and processes having set these complexes, rare gases were studied in ~300 rocks and mineral separates from 9 UACC, and concentrations of parent Li, K, U, and Th were measured in ~70 samples. $^4He/^3He$ ratios in He released by fusion vary from pure radiogenic values $\sim 10^8$ down to 6×10^4. The cosmogenic and extraterrestrial sources as well as the radiogenic production are unable to account for the extremely high abundances of ^3He, up to 4×10^{-9} cc/g, indicating a mantle-derived fluid in the Kola rocks. In some samples helium extracted by crushing shows quite low $^4He/^3He = 3 \times 10^4$, well below the mean ratio in mid ocean ridge basalts (MORB), $(8.9 \pm 1.0) \times 10^4$, indicating the contribution of ^3He-rich plume component. Magnetites are principal carriers of this component. Trapped ^3He is extracted from these minerals at high temperatures 1100°C to 1600°C which may correspond to decrepitation or annealing primary fluid inclusions, whereas radiogenic ^4He is manly released at a temperature range of 500°C to 1200°C, probably corresponding to activation of ^4He sites degraded by U, Th decay.

Similar $^4He/^3He$ ratios were observed in Oligocene flood basalts from the Ethiopian plume. According to a paleo-plate-tectonic reconstruction, 450 Ma ago the Baltica (including the Kola Peninsula) continent drifted not far from the present-day site of that plume. It appears that both magmatic provinces could relate to one and the same deep-seated mantle source.

The neon isotopic compositions confirm the occurrence of a plume component since, within a conventional $^{20}Ne/^{22}Ne$ versus $^{21}Ne/^{22}Ne$ diagram, the regression line for Kola samples is indistinguishable from those typical of plumes, such as Loihi (Hawaii). $^{20}Ne/^{22}Ne$ ratios (up to 12.1) correlate well with $^{40}Ar/^{36}Ar$ ones, allowing to infer a source $^{40}Ar/^{36}Ar$ ratio of about 4000 for the mantle end-member, which is 10 times lower than that of the MORB source end-member. In $(^3He/^{22}Ne)_{PRIM}$ versus $(^4He/^{21}Ne)_{RAD}$ plot the Kola samples are within array established for plume and MORB samples; almost constant production ratio of $(^4He/^{21}Ne)_{RAD} \cong 2 \times 10^7$ is translated via this array into $(^3He/^{22}Ne)_{PRIM} \sim 10$. The latter value approaches the solar ratio implying the non-fractionated solar-like rare gas pattern in a plume source.

The Kola UACC show systematic variations in the respective contributions of in situ-produced radiogenic isotopes and mantle-derived isotopes. Since these complexes were essentially plutonic, we propose that the depth of emplacement exerted a primary control on the retention of both trapped and radiogenic species, which is consistent with geological observations. The available data allow to infer the following sequence of processes for the emplacement and evolution of Kola Devonian UACC: 1) Ascent of the plume from the lower mantle to the subcontinental lithosphere; the plume triggered mantle metasomatism not later than ~700 to 400 Ma ago. 2) Metasomatism of the lithosphere (beneath the central part of the Kola Peninsula), including enrichment in volatile (e.g., He, Ne) and in incompatible (e.g., U, Th) elements. 3) Multistage intrusions of parental melts, their degassing, and crystallisation differentiation ~370 Ma ago. 4) Postcrystallisation migration of fluids, including loss of radiogenic and of trapped helium. Based on model compositions of the principle terrestrial reservoirs we estimate the contributions (by mass) of the plume material, the upper mantle material, and the atmosphere (air-saturated groundwater), into the source of parent melt at ~2%, 97.95%, and ~0.05%, respectively. *Copyright © 2002 Elsevier Science Ltd*

1. INTRODUCTION

Several reasons encourage studies of trace element and isotope systematics of ultrabasic-alkaline-carbonatites complexes (UACC). Petrologic (Le Bas, 1987; Wyllie et al., 1990), geochemical (Nelson et al., 1988) and isotopic (Andersen, 1987; Bell and Blenkinsop, 1989; Grunenfelder et al., 1986; Kwon et al., 1989) characteristics of UACC indicate clearly a mantle source for parent melts. Although the manifestations of alkaline and carbonatite magmatism observed at the earth surface are generally small, low-viscous carbonatite- and alkaline melts could have interacted with large volumes of the mantle. As a result, concentrations of some elements, such as Sr and REE, are rather high in

* Author to whom correspondence should be addressed (igor@inep.kolasc.net.ru).

the parent melts of alkaline and carbonatitic rocks when compared to crustal average abundances and these melts are able to provide trace-element and isotope characteristics of the mantle source with limited crustal contamination (Bell and Blenkinsop, 1989; Nelson et al., 1988; Woolley and Kempe, 1989).

Previous studies of the UACC have led to the following results relevant for this contribution:

1. The petrology and trace element geochemistry of UACC both indicate a metasomatically-processed volatile-element-enriched mantle source for the alkaline and carbonatite melts (Andersen, 1987; Hawkesworth et al., 1990; Kramm and Kogarko, 1994).
2. The isotopic signatures of UACC share similarities with oceanic island alkaline rocks suggesting similar sources and processes (Bell and Blenkinsop, 1989; Grunenfelder et al., 1986; Kwon et al., 1989; Nelson et al., 1988).

Because UAC parent melts have been enriched in volatile elements, they should contained large amounts of noble gases, so these important geodynamic tracers can be used to investigate the origin and evolution of the melts and the post magmatic development of the related intrusive bodies. However only a few relevant papers are available, except those related to the Kola UACC. Staudacher and Allegre (1982) first reported a small excess of ^{129}Xe in one carbonatite sample from Uganda, Africa. Later on Sasada et al. (1997) confirmed the excess and considered it as a primordial signature. These authors also reported high contributions of fission xenon isotopes (^{136}Xe/^{130}Xe ratios up to 1400) and nucleogenic Ne isotopes (^{20}Ne/^{22}Ne down to 0.01), which demonstrated the major role of crustal nuclear processes overwhelming mantle fingerprints.

In the case of the Devonian Kola UACC, Tolstikhin et al. (1985) reported MORB-like He, Ne, and Xe isotopic pattern for the least radiogenic samples. Mitrofanov et al. (1995), and Ikorsky et al. (1997) applied crushing extraction technique to the Kola samples and discovered quite low ^{4}He/^{3}He ratios, 60000, typical of plume materials. Marty et al. (1998) confirmed the plume-like isotope signatures by new He, Ne, and Ar isotope measurements. They showed that a good correlation between Ne and Ar isotopic ratios allowed one to propose that the ^{40}Ar/^{36}Ar ratio of the plume source was within 4000 to 6,000, an order of magnitude lower than the MORB convective mantle end-member. Recently Dauphas and Marty (1999) reported slightly positive δ^{15}N $\sim +3$ to $+5$ per mil relative to atmospheric N for nitrogen extracted by crushing from Kola minerals. These values are clearly different from the MORB end-member δ^{15}N value of -5 per mil.

This contribution presents new noble gas and parent trace element analyses obtained for 9 Devonian Kola ultrabasic alkaline carbonatite complexes (UACC) along with previously available data. The isotopic characteristics of trapped mantle fluid indicate solar-like isotopic signatures of light rare gases and allow us to identify a contribution of a rare gas plume component presumably originated in the lower mantle (hereafter plume component). Crushing and step-wise heating experiments were carried out in order to investigate sites of trapped and in situ produced isotopes in minerals. Finally magmatic and postmagmatic processes are discussed to shed light on behaviour of volatile species during settling of UAC complexes and 370 Ma long evolution afterwards.

2. GEOLOGICAL BACKGROUND

The Kola Alkaline Carbonatitic Province is situated in the north east part of the Baltic shield, which is composed predominantly by late Archaean tonalite-trondhjemite-granodiorite complexes younger than 2.95 Ga, and by subordinate supracrustal late Archaean—Early Proterozoic strata (Rundkvist and Mitrofanov, 1988). This region is divided into three megablocks, Karelian, Belomorian, and Kola (Kratz, 1978), which are interpreted as composite terrains finally settled $\sim$1.8 Ga ago (Balagansky et al., 1998).

Ultrabasic alkaline carbonatite complexes (UACC) are polyphase central-type bodies intruded, along with numerous dykes and pipes, Archaean and Early Proterozoic gneisses, granite-gneisses and granites (Fig. 1). The major UACC rock types are ultramafitolites, melilite-bearing rocks, foidolites, and carbonatites and/or multi-stage phoscorite-carbonatites. Ultramafitolites are olivine and/or olivine-clinopyroxene adcumulates with titanomagnetite, perovskite, amphibole, phlogopite, apatite and calcite in the intercumulus. Turjaites are the main type of melilite-bearing rocks. Foidolites form series of meso- and orthocumulates with variable quantities of clinopyroxene and nepheline (Kukharenko, 1967; Kogarko et al., 1995).

The Seblyavr complex (SB), briefly described below as an example, is situated in the north west part of Kola Peninsula (Fig. 1). The complex is a stock-like oval body intruding Archaean gneisses and having an exposed area of 4×5 km. The complex is characterised by a concentric zoning (Fig. 2). The core is composed by clinopyroxenites and olivinites, and is surrounded by a thin oval-like rim of nepheline clinopyroxenites and ijolite. Locally clinopyroxenites were transformed by pneumatolytic and autometasomatic processes into apatite-phlogopite-garnet-amphibole rocks and apatite clinopyroxenites (Kukharenko et al., 1965; Subbotin and Mihaelis, 1986). Phoscorites and carbonatites intruded the core during four stages, producing a concentric net of dykes and veins.

Rb-Sr, U-Pb, and Sm-Nd isochrones give crystallisation ages of 360 to 380 Ma, and 370 Ma is used hereafter as the mean age for the complexes (Amelin and Zaitsev, 1997; Bayanova et al., 1997; Kramm and Kogarko, 1994; Kramm et al., 1993; Zaitsev and Bell, 1995; Zaitsev et al., 1997).

The Dyke Complex (DC), more than 1000 dykes and explosion pipes, is situated mainly within a 250 km long belt along the northern coast of the White Sea (Fig. 1). The Kandalaksha Graben belonging to the regional Onega-Kandalaksha paleorift controls their emplacement (Beard et al., 1996, 1998). The dykes are characterised by 0.8 to 1.2 m thickness, up to 300 m length, and north to north-east orientation. According to field relationships, early and late dykes can be distinguished. Carbonatites, monticellite kimberlites, ultrabasic lamprophyres, and monchiquites compose the early dykes. These rocks contain lower crustal and host rock xenoliths (Vetrin and Kalinkin, 1992). Alkaline picrites, melanephelinites, nephelinites and alkaline syenite-porphyries compose the late dykes. Explosive pipes are associated with dykes. The typical rocks are foidites, melilitites, and olivine-phlogopite diamond-bearing kimberlites. Conventional and ^{40}Ar-^{39}Ar K-Ar dating gives 340 to 390 Ma ages for the dyke rocks (Kalinkin et al., 1993).

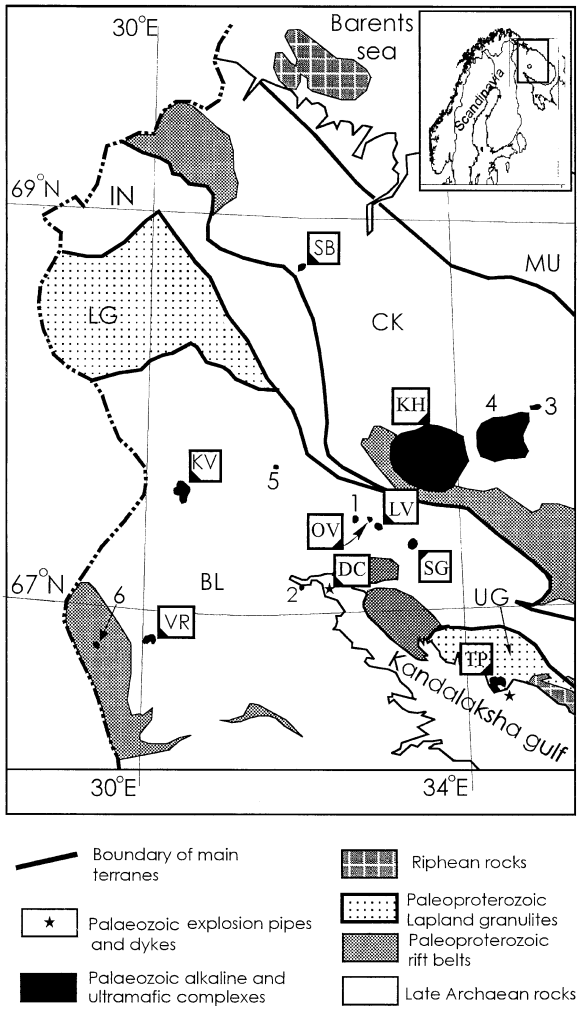

Fig. 1. Location of Palaeozoic alkaline and ultramafic-alkaline massifs in the Kola region. Investigated complexes: KH —Khibiny, KV —Kovdor, LV —Lesnaya Varaka, OV —Ozernaya Varaka, SB —Seblyavr, SG —Salmagora, TP —Turiy Peninsula, VR —Vuorijarvi, DC —Dyke complex. Other complexes: 1 —Afrikanda, 2 —Kandaguba, 3 —Kurga, 4 —Lovozero, 5 —Mavraguba, 6 —Sallanlatva. Dispersed terraines (fragments of a rifted Neoarchaean craton): MU —Murmansk, CK —Central Kola, BL —Belamorial, IN —Inari; accreted terranes (tectonic packages of Palaeoproterozoic island-arc formations) LG —Lapland Granulite, UG —Umba Granulite (Balagansky et al., 1998).

3. EXPERIMENTAL TECHNIQUES

The experimental techniques have already been discussed by Marty et al. (1998) and Tolstikhin et al. (1999a, 1999b) and are summarised below.

3.1. Rare Gas Measurements at Laboratory of Geochronology, Apatity, Russia

Two extraction lines for heating and crushing of samples were used (Kamensky et al., 1984; Ikorsky and Kusth, 1992). In both cases the extracted gases were admitted to an all-metal line and purified using Ti-Zr getters. The abundances of He and Ar isotopes were measured using a static mass spectrometer (MI 1201), which resolving power, $\sim$ 1000, allows complete separation of $^3He^+$ from $^3H^+$ and HD^+. The sensitivity for He was 5×10^{-5} A torr^{-1}, allowing measurements of $^4He/^3He$ ratios up to 10^8. The sensitivity for Ar was 3×10^{-4} A torr^{-1}. Mixture of pure ^3He, helium from a high-pressure tank ($^4He/^3He = 5 \times 10^7$) and air Ne, Ar, Kr and Xe was used as a standard for the calibration of the mass-spectrometer. The ratios $^4He/^3He = 6.29 \times 10^5$ and $^4He/^{20}Ne = 47$ in the mixture were measured using air as the primary standard in the Apatity laboratory; later on these ratios were verified at CRPG (Nancy). The concentrations were determined by the peak height method with an uncertainty of $\pm 5\%$ (1σ). Uncertainties in the $^4He/^3He$ ratios of $\sim 10^6$ and $\sim 10^8$ were 2 and 20%, respectively, and uncertainties in the $^{40}Ar/^{36}Ar$ ratios of 300 and 50000 were 0.3 and 25%, respectively. The analytical blanks were whithin 1×10^{-9}, 2×10^{-10}, and 1×10^{-10} cm^3 STP for ^4He, ^{20}Ne and ^{36}Ar, respectively, for both fusion and crushing experiments.

3.2. Rare Gas Measurements at CRPG, Nancy, France

Rare gases were extracted by vacuum crushing (Marty and Humbert, 1997; Marty et al., 1998; Richard et al., 1996). The released gases were cleaned over two Ti-sponge getters. After purification Ne and Ar were adsorbed on a stainless steel grid cooled at 17 K and He inlet into the analyser. ^4He and ^3He were measured using Faraday collector and electron multiplier, respectively. The He isotope ratios were normalised against a secondary standard, Irénée mineral spring gas, Réunion Island, 12.41 $\pm$ 0.09 Ra.

Neon was then desorbed from the cryogenic trap at 45 K and admitted into the mass spectrometer. The tube of the analyser comprises two SAES@ getters working at room temperature and a stainless steel finger containing active charcoal directly connected to the mass spectrometer ion source. This trap was cooled down to liquid nitrogen temperature 5 min before Ne admission and the gas was left in the mass spectrometer for 5 more minutes to minimize $^{40}Ar^{++}$, $^{20}NeH^+$, and CO_2^{++} interferences to Ne isotope peaks. Doing so, Ne isotope ratios for blanks were found to be within errors similar to that of standard Ne, and we did not apply interference corrections because, to our view, errors associated with determinations of single-charge/double-charge ratios were not competitive with respect to those associated with the very small contributions of double-charged species obtained in this procedure. The amount of Ne and its isotopic composition were determined by analysing Ne isotope masses during 12 cycles. The peak heights and the isotopic ratios were extrapolated to the time when counting started. After the measurements, the blank and mass discrimination corrections were applied.

Then Ar was desorbed from the cryogenic trap at 85 K, admitted into the mass spectrometer and analysed using the Faraday collector for ^{40}Ar, and electron amplification and ion counting for ^{36}Ar, ^{38}Ar (10 cycles). During these analyses, the ^{36}Ar blanks were typically 4×10^{-12} cc STP, and therefore small in comparison to the ^{36}Ar contents of the samples, representing only 0.2 to 4.0% of the total signals at mass 36.

3.3. U, Th, K and Li Measurements

The concentrations of U and Th were measured by X-radiography in Neva Expedition, St. Petersburg, Russia. The lowest

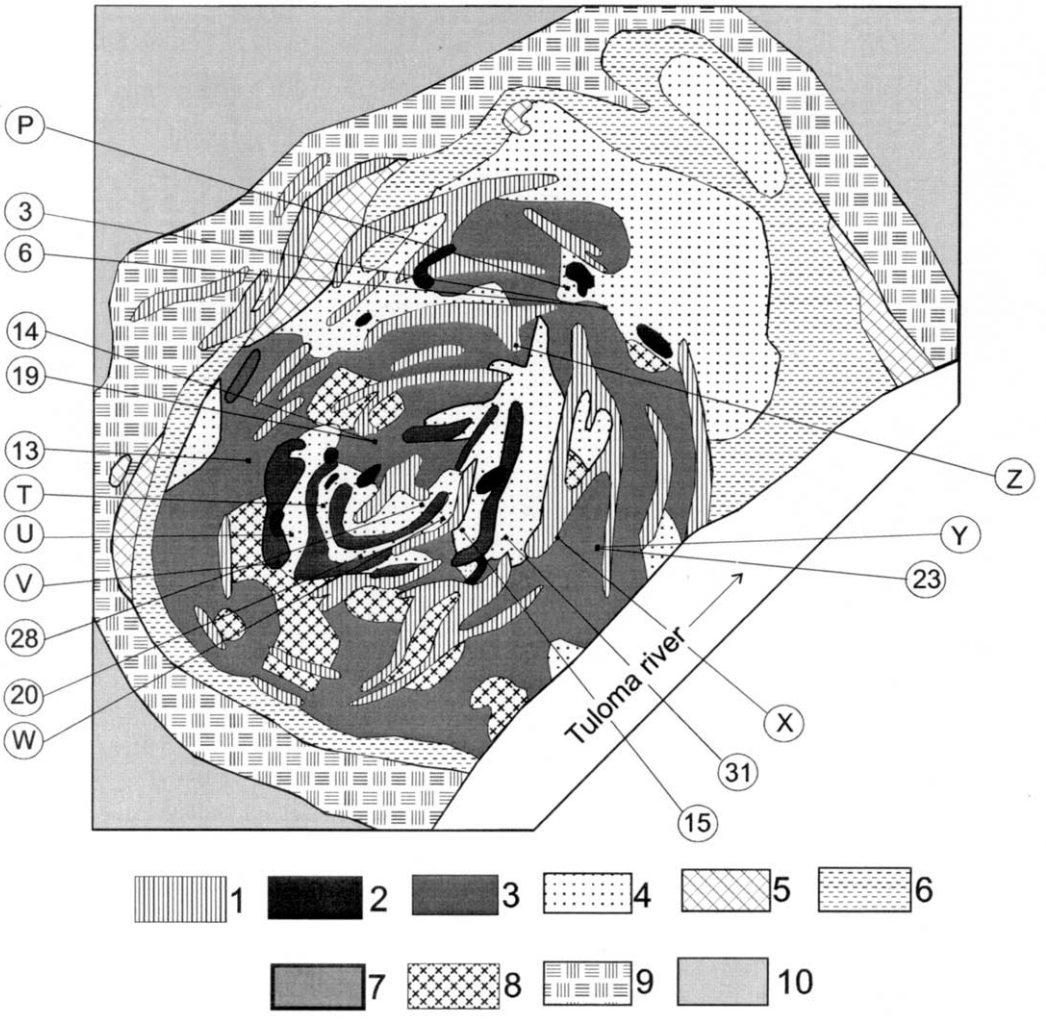

Fig. 2. Schematic geological map of Seblyavr complex (SB in Fig. 1, Subbotin and Michaelis, 1986, with simplifications).1 — carbonatites, 2 —phoscorites, 3 —apatite-phlogopite-diopside rocks, 4 —apatite-garnet-amphibole rocks and apatite clinopyroxenites, 5 —ijolites, 6 —nepheline clinopyroxenites, 7 — clinopyroxenites, 8 — ore-bearing clinopyroxenites and olivinites, 9 —fenites and fenitized gneisses, 10 — gneisses and migmatites. Sample sites (shown by point): square (rectangle)— outcrop, circle — borehole, number —number of sample (Tables 1 to 4), letter shows several samples at one and the same location; after slash — depth of a sample in borehole (m): 3/160, 6/70, 14/24, 19/336, 13/52, 28/353, 20/180, 15/350, 31/352, 23/132; P: 7/55, 8/55, 9/55, 10/55, 11/65; T: 32/250, 33/250, 34/250, 35/250, 36/19; U: 26/406, 30/325, 40/242; V: 37/243, 38/243, 39/243; W: 16/841, 17/841, 18/580, 21/930, 22/539, 24/462, 25/460, 27/467, 29/495; X: 4/82, 5/80; Y: 12/130, 23/132; Z: 1/49, 2/49. A more detailed description of the samples and complexes (including schematic maps with sampling sites) is available from preprint by Tolstikhin et al. (1999a, 1999b).

measurable concentration is ~0.5 ppm. K and Li were determined by spectrophotometry after acid attack and solution in distilled water in the Geological Institute, Apatity. The reproducibility of the analyses of these four elements was within ±10%.

4. RESULTS

4.1. Helium

Whole-rock (mineral) concentrations of ^{3}He and ^{4}He/^{3}He ratios vary within four orders of magnitude (Fig. 3). Ultramafic rocks present the highest ^{3}He concentrations observed in terrestrial samples, up to 4×10^{-9} cm^3 STP g^{-1} (sample SB-8, Table 1), and quite low ^{4}He/^{3}He ratios, down to $(6.4 \div 7.8) \times 10^4$ in samples SB-1 and LV-5. These values are noticeably below the mean MORB ratio $(8.9 \pm 0.9) \times 10^4$. The samples were mainly collected from boreholes or quarries, which rules out extraterrestrial sources or cosmogenic production on the Earth's surface (see Fig. 2). However, nuclear reactions could also produce He with low ^{4}He/^{3}He ratio in specific natural environments, and to identify trapped component of He, the measured concentrations He_M need be compared with those calculated for radiogenic in-situ produced He_C, assuming no gain/loss of species of interest. The concentrations of ^4He_C are calculated from measured U and Th concentrations (Table 1), and the age of the complexes, 370 Ma. Radiogenic ^{3}He origi-

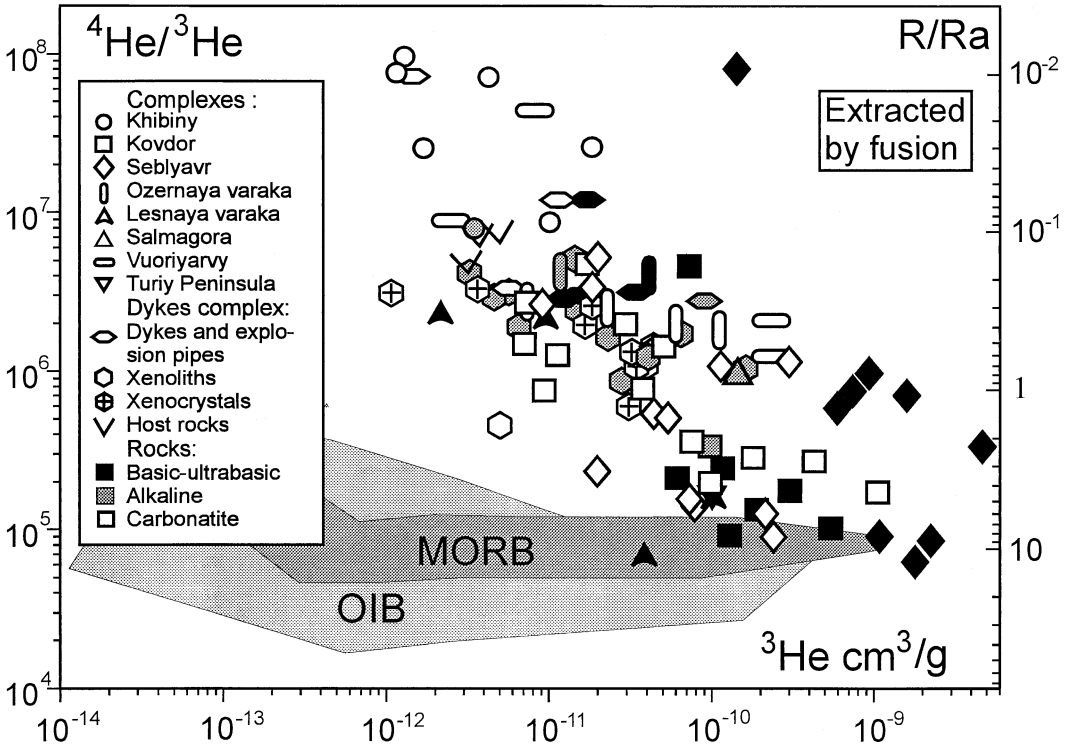

Fig. 3. Helium isotopes in samples from Kola ultrabasic-alkaline-carbonatite complexes: whole-rock data (He extraction by melting). Hereafter $R/Ra \equiv [(^3He/^4He)_{MEASURED}]/[(^3He/^4He)_{ATMOSPHERE}]$. Samples from Seblyavr (SB), Kovdor (KV) and Lesnaya Varaka (LV) show low $^4He/^3He$ ratios similar to or below the mean MORB ratio. ^3He abundances in some ultrabasic rocks and carbonatites from these complexes exceed those in MORB and OIB glasses. Sources of data for helium and neon (see Fig. 6 and 11) isotope abundances in MORB- and PLUME-related samples: Hiyagon et al. (1992), Honda et al. (1991, 1993), Kaneoka et al. (1986), Marty (1989), Moreira et al. (1995), Ozima and Zashu, (1983), Poreda and Farley (1992), Poreda and di Brozolo (1984), Sarda et al. (1985, 1988), Staudacher and Allegre (1989), Staudacher et al. (1986, 1989), Valbracht et al. (1996).

nates from the nuclear reaction $^6Li(n_t, \alpha)^3H$ (n_t stands for thermal neutron and α is the nucleus of ^4He) following by tritium decay $^3H \rightarrow \beta- \rightarrow {}^3He$ with the ^3H half life $\tau(^3H) = 12.2$ yr. The production of ^3He atom per ^4He atom depends on abundances of the major and some of the trace elements in a rock, the spatial distribution of U and Th and the Th/U ratios. Among trace elements, Li is the most important but Gd, Be, B also modify the flux of thermal neutrons. Morrison and Pine (1955) first proposed a method for estimation $^3He/^4He$ production ratio. Gorshkov et al. (1966) showed a good agreement, within 20%, between measured and calculated thermal neutron fluxes in natural rocks. Gerling et al. (1976) and Mamyrin and Tolstikhin (1984) compared measured and calculated $^3He/^4He$ ratios for different rocks and concluded that the measured ratios are mainly controlled by distribution of Li, U and Th among minerals and losses of helium isotopes from these minerals. Therefore, a direct comparison between measured and calculated ratios can not be used to calibrate ^3He_C calculations. Generally species releasing from rocks are accumulating in a complementary reservoir, groundwaters. In some cases it is possible to show that the host rocks were a major source of He isotopes for given aquifer. Providing high ^4He concentration in the groundwater (e.g., $\sim 10^{-2}$ cc STP/g) and, correspondingly, the long residence time of He in the aquifer, then validity of the calculated production $^4He/^3He$ ratio in rocks could be verified by measurements of this ratio in groundwaters. This approach illustrated similarity of measured and calculated ratios within ~50% (Tolstikhin et al., 1996). Even this poor accuracy is well enough to identify the ^3He source in KUACC as shown below.

All samples show $^4He_M/^4He_C \leq 1$, implying that an additional source for ^4He is not required. In contrast, $^3He_M/^3He_C$ ratios are extremely high in a great majority of samples, the average and maximum values being 4×10^3 and $\sim 10^5$, respectively, thus indicating a non-radiogenic, presumably mantle source for ^3He.

Combining crushing and step-wise heating experiments allow trapped helium to be (partially) separated from in situ produced He*. Generally, a substantial fraction of ^3He, ~40%, is extracted by crushing, whereas ^4He appears to reside mainly within a crystalline matrix (crushing releases only ~10% of ^4He). As a consequence, $^4He/^3He$ ratios are lower in helium extracted by crushing than in the bulk samples (compare Fig. 3 and 4). Concentrations of trapped helium isotopes vary in a wide range, similar to that observed for the whole-rock data. In a number of samples from different complexes $^4He/^3He$ ratios in trapped helium are substantially lower than the MORB ratio, indicating unambiguously a contribution of high-^3He plume-related fluid (Mitrofanov et al., 1995; Marty et al., 1998).

Table 1. Bulk He and Ar isotope abundances and U, Th, Li, and K concentrations

Sample	Rock/mineral	$^{3}He\ 10^{-12}$ cc/g	$^{4}He/^{3}He$ 10^{6}	$^{36}Ar\ 10^{-9}$ cc/g	$^{40}Ar/^{36}Ar$	U ppm	Th ppm	K % wt	Li ppm
KH	Khibiny								
KH-7	Foyaite	3.38	8.00	7.34	11400	3	11		
KH-8	Carbonatite	10.2	8.85	6.78	1250			0.35	17
KH-9	Carbonatite	18.4	26.3	22.0	662				
KH-12	Carbonatite	1.63	35.7	4.29	676	1	33	0.050	
KH-13	Carbonatite	1.12	76.9	3.29	607	1	70	0.040	
KH-14	Carbonatite	1.26	100.0	5.30	1850	1	19	0.26	
KH-15	Carbonatite	4.30	71.4	13.9	430				
KV	Kovdor								
KV-3	Dunite	305	0.18	3.56	2300	0.4	6	0.43	2.7
KV-4	Dunite	61.1	0.213	5.89	662	0.4	1	0.070	1.6
KV-5	Dunite	192	0.137	6.58	1740	0.6	1	0.25	2.8
KV-6	Dunite	129	0.092	3.79	3960				
KV-7	Dunite	69.9	4.88	5.08	7320				
KV-13	***Diopside*	111	0.246	9.97	632	2.3	0.5	0.085	0.0
KV-14	*+*Magnetite*	522	0.103	3.19	3500	0.8	0.5	0.058	7.8
KV-19	Ijolite	94.5	0.330	2.85	20700	0.7	3	3.2	1.0
KV-21	***Magnetite*	105	0.215	2.11	1650	0.8	0.5	0.018	1.0
KV-23	Phoscorite	36.6	0.781	10.0	848	1	1	0.016	
KV-24	Phoscorite	74.2	0.360	4.40	1500				
KV-27	Carbonatite	179	0.291	15.9	3090	2	5	2.5	
KV-28	Carbonatite	561	0.231	4.86	14600	2	6	3.2	
KV-29	**Clinopyroxene*	1050	0.181	2.33	7250				
KV-30	**Biotite*	7.04	1.56	3.14	50000				
KV-31	**Calcite*	11.3	1.3	17.3	7400				
KV-32	Carbonatite	435	0.28	6.03	10900	3	19	2.3	
KV-37	Carbonatite	9.40	0.79	5.96	1540			0.12	0.7
KV-41	Carbonatite	7.56	2.86	20.5	966	2	5	0.12	
KV-43	Carbonatite	49.3	1.43	9.04	1570	5	9	0.016	
KV-44	Carbonatite	17.4	5.08	2.61	2100			0.14	0.2
KV-46	Carbonatite	29.3	1.98	3.20	3310				
SB	Sebl'yavr								
SB-1	Dunite	1716	0.064	10.8	808	1.4	3	0.45	4.6
SB-3	Dunite	1050	0.085	3.47	3340	1.1	4	0.52	2.0
SB-5	Dunite	730	0.714	3.09	1680	18	16	0.23	2.2
SB-6	Clinopyroxenite	1980	0.078	5.22	1850	3	6	0.48	2.2
SB-7	Clinopyroxenite	1480	0.680	3.75	2290	4	51	0.15	1.2
SB-8	**Magn. fraction*	4290	0.334	4.99	2180				
SB-9	**Clinopyroxene*	591	0.575	3.10	1640				
SB-10	**Perovskite*	129	76.9	5.68	687				
SB-13	Clinopyroxenite	842	0.862	6.03	1690	10	47	0.74	2.2
SB-15	Phoscorite	112	1.09	5.61	4930	8	24	2.13	2.2
SB-17	Phoscorite	299	1.15	2.87	3540	6.1	27	1.97	5.8
SB-22	Carbonatite	18.4	3.39	11.4	1430	2.6	9.1	0.39	2.4
SB-23	Carbonatite	19.8	5.15	9.02	1400			0.19	4.5
SB-26	Carbonatite	8.99	2.66	19.5	584	5.1	20	0.41	2.1
SB-32	Carbonatite	214	0.126	8.99	801				
SB-33	**Pyrrhotite*	19.3	0.233	2.35	383				
SB-34	**Dolomite*	240	0.089	106.3	349				
SB-35	**Ankerite*	53.5	0.505	9.98	952				
SB-36	Carbonatite	44.0	0.539	3.55	1220	1	16	0.008	
SB-37	Carbonatite	77.3	0.150	3.31	936	0.5	9	0.057	3.4
SB-40	Carbonatite	74.3	0.157	5.83	721	0.5	2	0.062	3.2
	Ozernaya								
OV	Varaka								
OV-6	Clinopyroxenite	42.1	3.92	4.64	3900	1.9	12	0.53	3.1
OV-11	Ijolite	12.1	4.37	5.37	6920	0.7	7.1	2.0	1.9
OV-15	Carbonatite	59.7	1.96	7.71	1890	1	5	0.040	
OV-16	**Clinopyroxene*	110	1.78						
OV-17	**Calcite*	22.3	2.53	16.5	885				
OV-19	Carbonatite	7.28	2.67	5.54	4040	1	10	0.19	1.3
LV	Lesnaya Varaka								
LV-1	Dunite	79.0	0.172	5.41	665	0.5	3	0.021	2.2
LV-5	**Ti-magnetite*	37.9	0.069	1.54	2930				
LV-2	Dunite	9.68	2.22	4.57	394	0.1	1.3	0.018	1.1
LV-4	**Olivine*	2.14	2.38	2.67	1430				

(Continued)

Table 1. (Continued)

Sample	Rock/mineral	$^{3}He\ 10^{-12}$ cc/g	$^{4}He/^{3}He$ 10^{6}	$^{36}Ar\ 10^{-9}$ cc/g	$^{40}Ar/^{36}Ar$	U ppm	Th ppm	K % wt	Li ppm
SG	Salmagora								
SG-20	Turjaite	139.0	0.97	3.61	5310			0.73	2.2
VR	Vuorijarvi								
VR-1	Dunite	242	2.02	5.01	3370				
VR-17	Carbonatite	2.53	9.09	11.2	2140			0.68	4.3
VR-22	Carbonatite	8.19	47.62	6.39	3770			0.20	0.5
VR-26	Carbonatite	248	1.27	10.5	1260			0.083	8.8
	Turiy								
TP	Peninsula								
TP-7	Turjaite	99.5	0.161	3.03	4450				
DC	Dyke Complex								
DC-1	Lamprophyre	11.7	2.94	18.7	2500	5	7	1.81	80.0
DC-2	**Amphibole*	32.6	1.33	7.30	3390	0.2	6	1.32	9.0
DC-3	**Amphibole*	33.2	1.23	8.93	2800	1	5	1.24	9.0
DC-4	Lamprophyre	15.3	2.94	8.14	9210			1.51	
DC-5	Lamprophyre	16.5	11.8	8.28	3790	5.1	24	1.37	37.0
DC-6	**Amphibole*	34.3	1.05	3.22	4780	0.4	5	1.06	4.0
DC-7	**Amphibole*	39.8	1.06	3.67	4900	0.3	5	0.98	40.0
DC-12	Carbonatite	10.9	12.5	17.76	2790	0.9	6	2.1	4.0
DC-13	**Amphibole*	3.54	3.39	10.4	2230	0.4	6	1.1	12.0
DC-14	Kimberlite	33.9	3.12	13.5	1350	2.3	16	0.75	8.0
DC-18	Nephelinite	85.3	2.77	11.2	2670	6.1	5	1.3	12.0
DC-19	**Amphibole*	43.2	1.39	3.35	9240	1	8	1.7	7.0
DC-21	**Amphibole*	5.58	3.11	5.33	3390	0.6	7	1.3	73.0
DC-22	Granulite	6.42	1.93	3.21	4360	0.2	3	0.69	15.0
DC-23	Granulite	4.62	3.03	11.5	1380			0.48	
DC-24	Granulite	3.23	3.96	4.26	6540	0.2	3	1.7	5.0
DC-25	**Garnet*	1.05	3.04	1.06	1220				
DC-26	**Pyroxene*	17.6	2.49	5.90	2424	0.3	1	0.14	17.0
DC-28	Granulite	14.7	5.08	8.12	3080				
DC-30	Granulite	15.2	2.47	13.3	1370				
DC-33	Carbonatite	1.43	71.4	4.92	4270	10	23	1.3	30.0
DC-37	Carbonatite	4.84	0.455	4.94	2570	0.2	3	0.65	2.0
DC-40	Carbonatite	44.4	1.35	12.6	2260	2.2	4	1.8	47.0
DC-41	**Amphibole*	30.7	0.595	8.89	2920	1	13	1.2	3.0
DC-42	***Amphibole*	16.9	2.01	5.42	6990	1.5	13	2.3	78.0
DC-44	Amphibolite	162	1.02	3.67	6480			1.6	
DC-45	Amphibolite	28.3	0.847	3.63	7710	0.4	25		26.0
DC-46	Amphibolite	23.2	1.64	12.9	2940			1.2	
DC-47	Amphibolite	3.08	4.81	7.90	9600	0.3	3	1.6	10.0
DC-48	Amphibolite	4.88	7.81	5.45	11900	0.3	3	0.78	10.0
DC-49	Amphibolite	3.63	7.52	5.82	18200	1.1	8	0.98	12.0
DC-50	Pyroxenite	38.1	1.23	8.38	2730	0.5	7	0.14	18.0
DC-51	Pyroxenite	65.5	1.695	3.84	5210	0.4	4		5.0
DC-52	Pyroxenite	17.1	2.04	3.32	6030	0.7	5	1.0	30.0
DC-54	Metasomatite	35.5	1.27	7.99	4480	0.7	12	0.64	20.0
DC-55	Metasomatite	5.61	3.03	13.8	1380	0.3	8	0.60	27.0

* Mineral separated from a rock sample listed above.
** Parentless mineral.

Dunite SB-1 from the Seblyavr massif and magnetic fraction SB-2 separated from this rock show the lowest $^{4}He/^{3}He = (3.02 \pm 0.01) \times 10^{4}$. The ^{3}He concentration of the magnetic fraction exceeds by a factor of 4.5 that in the parent rock, but $^{4}He/^{3}He$ ratios are indistinguishable (Table 2).

4.2. Parent—Daughter Relationships

The $^{4}He/^{3}He$ range is becoming narrower with increasing ^{3}He (Fig. 3, 4), as expected from dilution of a mantle end-member by radiogenic component. However, samples with high ^{3}He contents still show $^{4}He/^{3}He$ varying within a factor of ~20. The U-Th-He relationships allow distinguishing whether the initial $^{4}He/^{3}He$ ratio in a magmatic fluid was heterogeneous or postmagmatic processes set this variability of He isotope compositions. The U and Th concentrations (Table 1) are generally high, up to 20 ppm, and 70 ppm, respectively, by a factor of ~100 higher than those typical of ultramafic rocks (Taylor and McLennan, 1985). For the given age, 370 Ma, the radiogenic $^{4}He^{*}$ production is proportional to the sum of U and 0.24Th (Zartman et al., 1961). Providing a closed system evolution the data points should lie on the reference evolution line having slope of $^{4}He/(U+0.24Th) = 45\ cm^{3}\ g^{-1}$ (solid line in Fig. 5). Several data-points approach this line but generally they scatter below, indicating the open system behaviour. Most

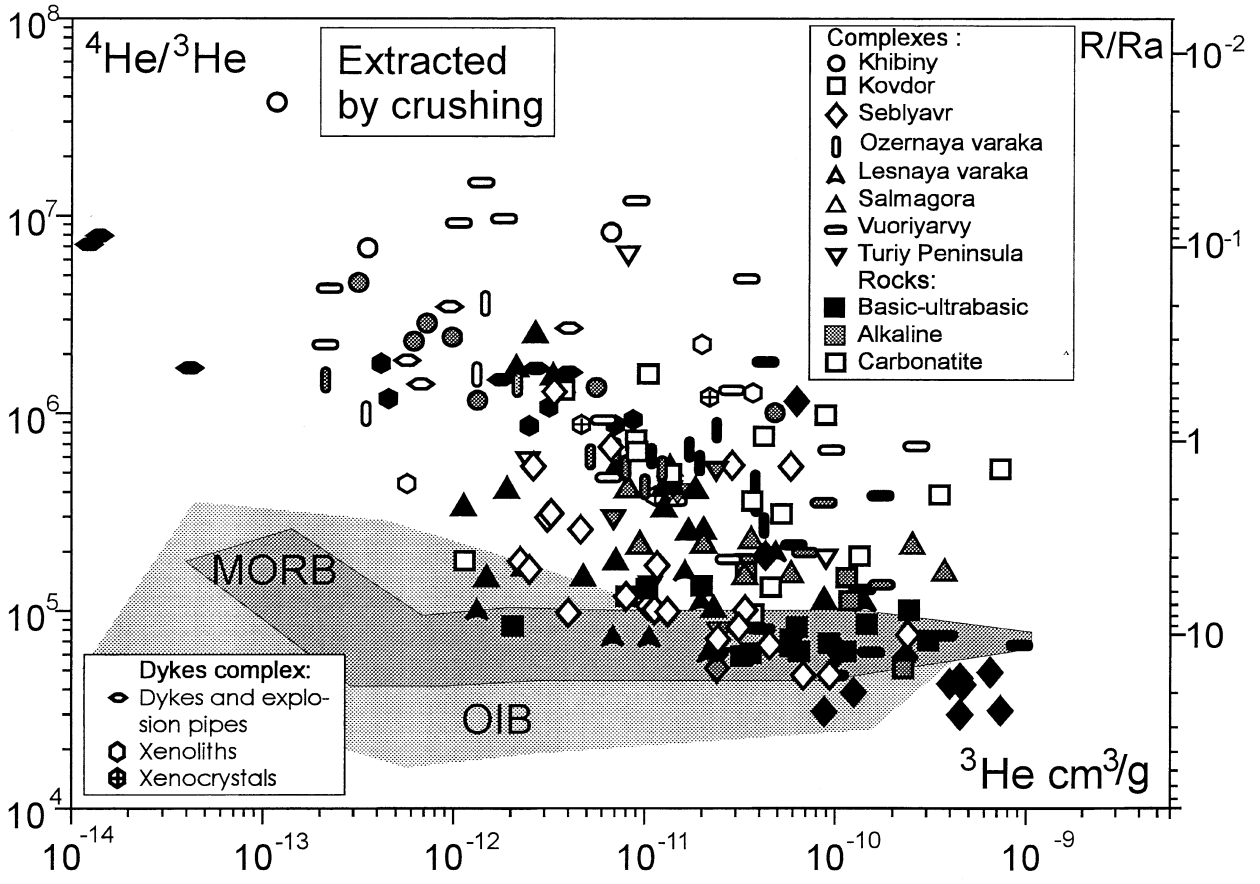

Fig. 4. Helium isotopes in samples from Kola ultrabasic-alkaline-carbonatite complexes: fluid component (He extraction by crushing). Both $^4He/^3He$ ratios and especially ^3He concentrations in vesicles vary within a great range. The lowest ratios are well below MORB values indicating a contribution of high-^3He plume component (see Fig. 3 for sources of MORB and OIB data).

likely this is due to helium loss that is typical of both igneous and sedimentary rocks (Mamyrin and Tolstikhin, 1984; Tolstikhin et al., 1996). Importantly, several data-points, having low $^4He/^3He$ and $(U+0.24Th)/^3He$ ratios, are close to the evolution line, implying a limited loss and a narrow interval for $^4He/^3He$ ratios in trapped He.

To estimate the initial ratios, these samples are presented in a linear co-ordinate plot (inset in Fig. 5). The regression line gives the mean $^4He/^3He = 30000$ for the Kola plume, which is indistinguishable from (i) the lowest measured value in He released by crushing (samples SB-1 and SB-2, Table 2) and (ii) from the initial ratio confined by the reference evolution line. The three independent approaches appear to be self-consistent. The error envelope indicates range of possible initial ratios, which are below the mean MORB ratio, 89000 (Tolstikhin and Marty, 1998), and overlap the lowest plume value, 20000 (36 Ra; Honda et al., 1993). This range is much narrower than that seen in Figure 3 and 4.

4.3. Neon and He-Ne Relationships

The conventional three-isotope plot (Fig. 6) shows a good correlation between $^{21}Ne/^{22}Ne$ and $^{20}Ne/^{22}Ne$ ratios in neon extracted by crushing (Marty et al., 1998). $^{20}Ne/^{22}Ne$ ratios vary from 10.5 to 12.1 (Table 3) reflecting mixing between the atmospheric (9.8) and the solar (13.7) neon (Honda et al., 1991, 1993). The slope of the regression line for Kola samples (only data for Ne extracted by crushing were regressed), SR(Kola) = 190 ± 40, is slightly below that observed for Loihi samples, SR(Loihi) = 250 ± 25, but well above SR(MORB) = 90 ± 4, emphasizing the occurrence of a plume rare gas component. Moreover, the slope would have been even steeper if 370 Ma old Kola samples were corrected for in-situ produced radiogenic Ne.

Indeed, measured $(^4He/^3He)_M$ ratios in all samples plotted in Figure 6 exceed $(^4He/^3He)_{PLUME}$ (Fig. 5, Tables 1,2) indicating a contribution of radiogenic helium isotopes, and similar effect is expected for neon. A plausible candidate for the pure nucleogenic end-member R appears to be Ne from Khibiny carbonatites; 5 of these rocks, containing pure radiogenic He, give average $^{20}Ne/^{22}Ne = 5.3$ and $^{21}Ne/^{22}Ne = 0.1$ (Tolstikhin et al., 1985). These values reflect the high fluorine contents of Kola UACC, and therefore an enhanced contribution of radiogenic ^{22}Ne from reaction $^{19}F(\alpha, n)^{22}Na \xrightarrow{\beta+} {}^{22}Ne$.

Data-points R and M (sample KV-28, Table 3, as an exam-

Table 2. He isotope abundances in vesicles

Sample	Rock/mineral	$^3He\ 10^{-12}$ cc/g	$^4He/^3He$ 10^6	Sample	Rock/mineral	$^3He\ 10^{-12}$ cc/g	$^4He/^3He$ 10^6
KH	Khibiny			LV	Lesnaya Varaka		
KH-1	Foyaite	1.0	2.38	LV-1	Dunite	32.5	0.086
KH-2	Foyaite	5.5	1.34	LV-2	Dunite	6.7	0.074
KH-3	Foyaite	0.7	2.85	LV-3	Dunite	10.2	0.072
KH-4	Foyaite	46.8	1.02	LV-4	**Olivine*	1.3	0.101
KH-5	Foyaite	0.3	4.54	LV-5	**Ti-magnetite*	21.2	0.061
KH-6	Foyaite	0.6	2.32	LV-6	***Ti-magnetite*	48.5	0.196
KH-7	Foyaite	1.3	1.16	LV-7	***Ti-magnetite*	141.1	0.110
KH-8	Carbonatite	6.4	8.19	LV-8	***Clinopyroxene*	19.7	0.112
KH-10	Carbonatite	0.4	6.84	LV-9	***Ti-magnetite*	16.0	0.156
KH-11	Carbonatite	0.1	37.0	SG	Salmagora		
KV	Kovdor			SG-1	Dunite	1.5	0.144
KV-1	Dunite	32.1	0.06	SG-2	Dunite	2.3	0.167
KV-2	Dunite	64.2	0.064	SG-3	Dunite	18.0	0.427
KV-3	Dunite	91.6	0.068	SG-4	Dunite	2.6	2.55
KV-4	Dunite	34.8	0.060	SG-5	**Olivine*	1.1	0.346
KV-5	Dunite	109	0.063	SG-6	**Ti-magnetite*	2.1	1.71
KV-8	Dunite	10.1	0.129	SG-7	Dunite	6.9	0.552
KV-9	Dunite	2.0	0.084	SG-8	Dunite	3.3	1.56
KV-10	Dunite	62.0	0.084	SG-9	Dunite	1.9	0.424
KV-11	Clinopyroxenite	239	0.100	SG-10	Dunite	12.3	0.334
KV-12	Clinopyroxenite	145	0.086	SG-11	Dunite	7.0	0.186
KV-13	***Diopside*	57.8	0.074	SG-12	Dunite	21.5	0.107
KV-14	***Magnetite*	298	0.071	SG-13	Dunite	13.5	0.526
KV-15	Melilitolite	55.7	0.068	SG-14	Dunite	13.6	0.418
KV-16	Melilitite	19.8	0.132	SG-15	Clinopyroxenite	86.4	0.113
KV-17	Turjaite	221	0.051	SG-16	Clinopyroxenite	4.7	0.148
KV-18	Ijolite	114	0.148	SG-17	Clinopyroxenite	19.6	0.260
KV-19	Ijolite	33.7	0.152	SG-18	Clinopyroxenite	12.4	0.444
KV-20	Ijolite	116	0.111	SG-19	Clinopyroxenite	16.5	0.254
KV-21	***Magnetite*	44.4	0.132	SG-20	Turjaite	56.5	0.157
KV-22	Phoscorite	7.9	0.120	SG-21	Turjaite	354	0.158
KV-24	Phoscorite	35.2	0.097	SG-22	Turjaite	245	0.212
KV-25	Phoscorite	49.6	0.318	SG-23	Melteygite	9.3	0.218
KV-26	Phoscorite	86.0	1.00	SG-24	Ijolite-melteygite	13.0	0.408
KV-33	Carbonatite	13.2	0.476	SG-25	Ijolite-melteygite	19.8	0.222
KV-34	Carbonatite	3.8	1.32	SG-26	Ijolite-melteygite	7.9	0.417
KV-35	Carbonatite	9.2	0.633	SG-27	Ijolite	34.1	0.148
KV-36	Carbonatite	35.3	0.360	SG-28	Ijolite	34.6	0.231
KV-37	Carbonatite	1.1	0.179	SG-29	Carbonatite	55.4	0.527
KV-38	***Magnetite*	133	0.195	SG-30	Carbonatite	26.5	0.521
KV-39	***Calcite*	336	0.398	VR	Vuorijarvi		
KV-40	Carbonatite	9.0	0.714	VR-1	Dunite	42.0	0.145
KV-42	Carbonatite	710	0.526	VR-2	Dunite	93.9	0.048
KV-44	Carbonatite	10.0	1.61	VR-3	Dunite	40.9	0.083
KV-45	Carbonatite	39.7	0.781	VR-4	Dunite	34.9	0.083
SB	Sebl'yavr			VR-5	Dunite	56.8	0.063
SB-1	Dunite	85.9	0.030	VR-6	Clinopyroxenite	170	0.376
SB-2	**Magn.fraction*	405	0.030	VR-7	***Ti-magnetite*	42.0	1.79
SB-3	Dunite	120	0.036	VR-8	Clinopyroxenite	148	0.063
SB-4	Dunite	40.8	0.179	VR-9	Clinopyroxenite	360	0.074
SB-5	Dunite	98.1	0.060	VR-10	**Clinopyroxene*	60.0	0.213
SB-6	Clinopyroxenite	694	0.031	VR-11	**Ti-magnetite*	907	0.067
SB-7	Clinopyroxenite	412	0.045	VR-12	Clinopyroxenite	134	0.126
SB-8	**Magn,fraction*	601	0.046	VR-13	Ijolite	186	0.152
SB-9	**Clinopyroxene*	388	0.042	VR-14	Ijolite-urtite	66.5	0.191
SB-10	**Perovskite*	59.8	1.099	VR-15	Ijolite	78.1	0.352
SB-11	Clinopyroxenite	215	0.055	VR-16	Ijolite-urtite	32.4	0.188
SB-12	Clinopyroxenite	424	0.041	VR-17	Carbonatite	0.2	2.21
SB-13	Clinopyroxenite	429	0.040	VR-18	Carbonatite	14.1	0.355
SB-14	Ijolite	23.6	0.051	VR-19	Carbonatite	27.6	0.181
SB-15	Phoscorite	66.3	0.047	VR-20	Carbonatite	8.9	11.8
SB-16	Phoscorite	4.4	0.248	VR-21	Carbonatite	1.7	9.71
SB-17	Phoscorite	89.4	0.045	VR-22	Carbonatite	1.0	9.09
SB-18	Phoscorite	7.8	0.113	VR-23	Carbonatite	0.2	4.29

(Continued)

Table 2. (Continued)

Sample	Rock/mineral	^{3}He 10^{-12} cc/g	^{4}He/^{3}He 10^6	Sample	Rock/mineral	^{3}He 10^{-12} cc/g	^{4}He/^{3}He 10^6
SB-19	Phoscorite	32.5	0.099	VR-24	Carbonatite	29.0	1.31
SB-20	Carbonatite	11.3	0.159	VR-25	Carbonatite	95.1	0.662
SB-21	Carbonatite	2.1	0.172	VR-26	Carbonatite	250	0.696
SB-22	Carbonatite	10.4	0.101	VR-27	Carbonatite	5.9	0.917
SB-23	Carbonatite	2.5	0.518	VR-28	Carbonatite	1.3	14.7
SB-24	Carbonatite	3.0	0.294	TP	Turiy Peninsula		
SB-25	Carbonatite	3.1	0.304	TP-1	Clinopyroxenite	24.5	0.057
SB-26	Carbonatite	3.3	1.23	TP-2	Clinopyroxenite	10.3	0.136
SB-27	Carbonatite	2.4	0.154	TP-3	Clinopyroxenite	24.1	0.079
SB-28	Carbonatite	6.3	0.637	TP-4	Turjaite	14.6	0.389
SB-29	Carbonatite	229	0.073	TP-5	Turjaite	6.7	0.305
SB-30	Carbonatite	10.9	0.097	TP-6	Turjaite	23.0	0.521
SB-31	Carbonatite	12.6	0.095	TP-7	Turjaite	24.8	0.081
SB-37	Carbonatite	23.5	0.070	TP-8	Carbonatite	2.4	0.551
SB-38	**Pyrrhotite*	3.9	0.096	TP-11	Carbonatite	85.7	0.186
SB-39	**Dolomite*	43.4	0.064	TP-12	Carbonatite	7.7	6.49
SB-40	Carbonatite	29.7	0.077	DC	Dyke Complex		
OV	Ozern. Varaka			DC-3	**Amphibole*	4.6	0.87
OV-1	Clinopyroxenite	23.5	0.809	DC-8	Lamprophyre	4.0	1.58
OV-2	Clinopyroxenite	38.2	0.345	DC-9	Lamprophyre	3.5	1.31
OV-3	Clinopyroxenite	18.5	0.556	DC-10	Lamprophyre	2.6	1.69
OV-4	**Clinopyroxene*	17.1	0.654	DC-11	Lamprophyre	1.7	1.49
OV-5	**Ti-magnetite*	37.0	0.441	DC-15	Kimberlite	72	7.69
OV-6	Clinopyroxenite	41.6	0.265	DC-16	Kimberlite	138	7.94
OV-7	Clinopyroxenite	10.5	0.564	DC-17	Kimberlite	385	1.82
OV-8	Ijolite	9.7	0.435	DC-19	**Amphibole*	21.6	1.22
OV-9	Ijolite	12.0	0.518	DC-27	Granulite	7.1	0.893
OV-10	Ijolite	7.0	0.633	DC-28	Granulite	2.4	0.893
OV-11	Ijolite	5.1	0.588	DC-29	Granulite	8.4	0.943
OV-12	Ijolite-urtite	7.3	0.549	DC-30	Granulite	3.1	1.09
OV-13	Syenite	2.1	1.38	DC-31	Granulite	0.4	1.8
OV-14	Syenite	0.2	1.44	DC-32	Carbonatite	0.7	1.41
OV-18	Carbonatite	0.3	0.952	DC-34	Carbonatite	19.6	2.1
OV-19	Carbonatite	1.3	1.58	DC-35	Carbonatite	0.6	0.431
OV-20	Carbonatite	1.4	3.66	DC-36	Carbonatite	36.6	1.26
				DC-38	Carbonatite	1.0	3.57
				DC-39	Carbonatite	0.6	1.85
				DC-41	**Amphibole*	11.4	0.376
				DC-43	Carbonatite	4.1	2.75
				DC-53	Pyroxenite	0.4	1.18

See Footnote to Table 1.

ple) determine the mixing line JPMR, which also crosses the Solar-Air mixing line at point J and passes through a yet unknown plume-related composition P. Departure of a data-point from the "juvenile" composition J (having no in situ produced nucleogenic components) to the right along JPMR is proportional to the addition of radiogenic Ne*. The proportion

$$[(^{21}Ne/^{22}Ne)_P - (^{21}Ne/^{22}Ne)_J]/[(^{21}Ne/^{22}Ne)_M - (^{21}Ne/^{22}Ne)_J] \approx$$

$$[(^4He/^3He)_P - (^4He/^3He)_{PRIM}]/[(^4He/^3He)_M - (^4He/^3He)_{PRIM}] \approx 0.11 \quad (1)$$

corresponds to JP/JM ratio and gives the composition P of plume-related Ne, in sample KV-28 (Tables 1, 3). This proportion relies on known $(^4He/^3He)_P = 30000$, $(^4He/^3He)_{PRIM} = 2200$ (Geiss, 1993, Section 5.3), and the constant production $^4He^*/^{21}Ne^*$ (Section 5.3). Radiogenic $^4He^*$ and $^{21}Ne^*$ were produced within radiation damage tracks controlling their migration through minerals. Therefore a similar rate of loss is assumed for both isotopes.

The corrected compositions generate a distinct array (Fig. 6). The regression gives slope SR(Kola, corrected) = 310 ± 50, which is even somewhat steeper than SR(Loihi), whereas the initial Kola He is more radiogenic than helium in Loihi. The corrected Kola data resemble He-Ne relationships discussed recently by Dixon et al. (2000): basalt glasses and olivines from Reykjanes Ridge, Iceland, show more primitive Ne and more radiogenic He than the Loihi samples. Even though the correction is imprecise, the corrected He-Ne systematics suggests the occurrence of a very primitive plume component of neon even in samples having substantial contributions of in situ produced

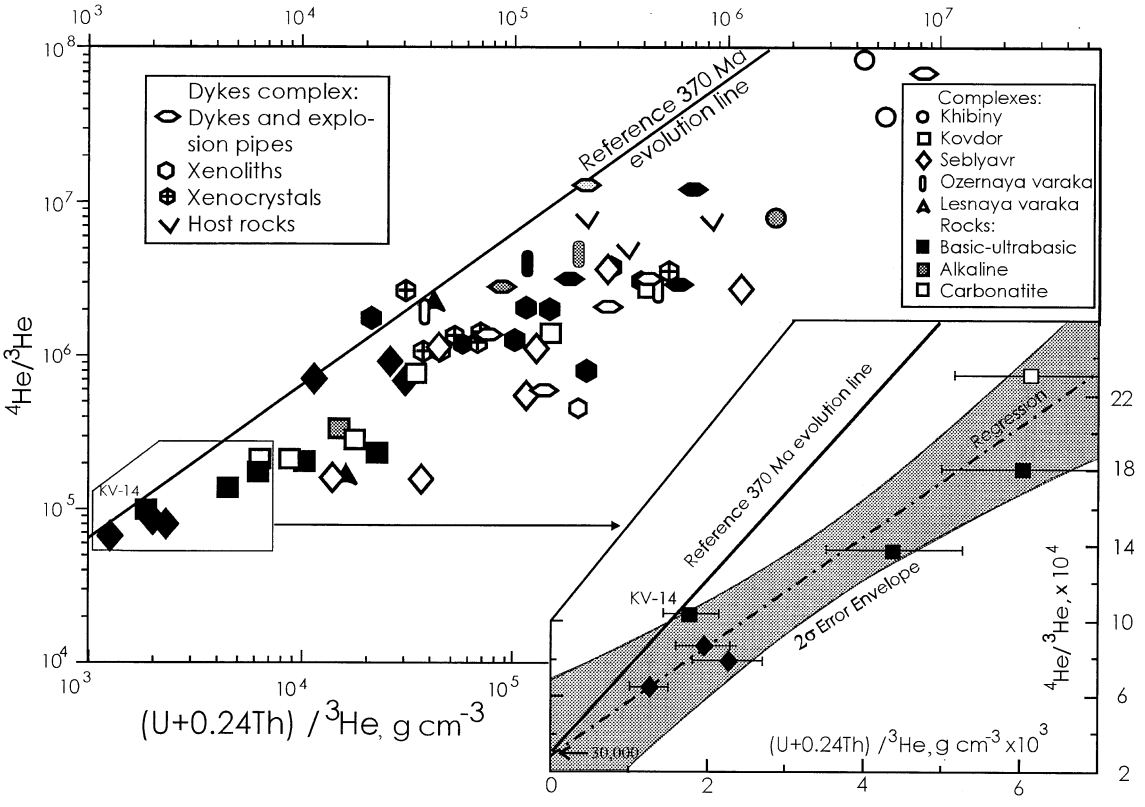

Fig. 5. Relationships between whole-rock abundances of parent and daughter species. He was extracted by fusion. Error-bars for $^4He/^3He$ ratios (inset) are within the size of symbols. Most samples lay below the reference evolution line indicating a partial loss of helium. Inset comprises samples with low $(U+0.24Th)/^3He$ and $^4He/^3He$ ratios. The regression line (inset) indicates the $^4He/^3He$ ratio, which is the same as the lowest measured ratio in helium extracted by crushing (samples SB-1, SB-2, and SB-6, Table 2). Error envelope shows the range of initial ratios within 95% confidence interval. The reference evolution line touches sample KV-14 within the bi-logarithmic plot. Co-ordinates of this sample (Table 1) and the slope (45, corresponding to 370 Ma age) set this line within the linear co-ordinate plot (inset), and the intercept gives the initial ratio similar to that inferred above from the regression and measurements.

nuclides. More work is needed to improve accuracy of this correction, and Kola UAC samples having quite high concentrations of trapped species appears to be suitable for this work.

4.4. Argon and Lighter Rare Gases

The inventory of Ar isotopes shows that three sources are significant: atmospheric Ar, in-situ radiogenic $^{40}Ar^*$, and trapped Ar. $^{40}Ar/^{36}Ar$ ratios in Ar extracted by crushing vary by an order of magnitude, from the air value of 296 to $\approx$ 3000, implying a substantial contribution of atmospheric Ar in the trapped fluid. In a conventional $^{40}Ar/^{36}Ar$ versus $K/^{36}Ar$ diagram, the data-points mainly cluster around the reference 370 Ma evolution line crossing the $^{40}Ar/^{36}Ar$ axis at the atmospheric ratio (Fig. 7). However, several Kovdor samples are above the evolution line, suggesting an initially elevated $^{40}Ar/^{36}Ar$ of $\sim$4000. Samples having low $K/^{36}Ar$ ratios (inset in Fig. 7) also point to an initial $^{40}Ar/^{36}Ar$ ratio well above the atmospheric value.

A good correlation between $^{20}Ne/^{22}Ne$ and $^{40}Ar/^{36}Ar$ allows an independent estimate for the initial $^{40}Ar/^{36}Ar$ ratio. This correlation, resulting from mixing between atmospheric and mantle components, shows definitely that the mantle end-member must have $^{40}Ar/^{36}Ar > 3000$, most likely within 4000 to 6000 (Marty et al., 1998).

5. DISCUSSION

5.1. Warehouses of Mantle Fluid: Inclusions and Host Minerals

To identify the sites of the trapped fluids, olivines, pyroxenes and magnetites were separated from ultrabasic rocks, having high abundances of trapped He (Table 4). The observed sequence of ^3He concentrations follows the crystallisation order, and the latest crystallised Ti-magnetite acquires the highest concentration. Since rare gases are incompatible elements (e.g., Marty and Lussiez, 1993), a 10-fold ^3He enrichment is expected in the last 10% fraction of basic melt (from which the magnetite was crystallised), providing retention of volatiles in the course of crystallisation. Indeed products of late-magmatic activity, such as meter-size crystals of clinopyroxenes and phlogopites, observed in the Kovdor (Kukharenko et al., 1965), indicate a remarkable retention of fluids. The occurrence of

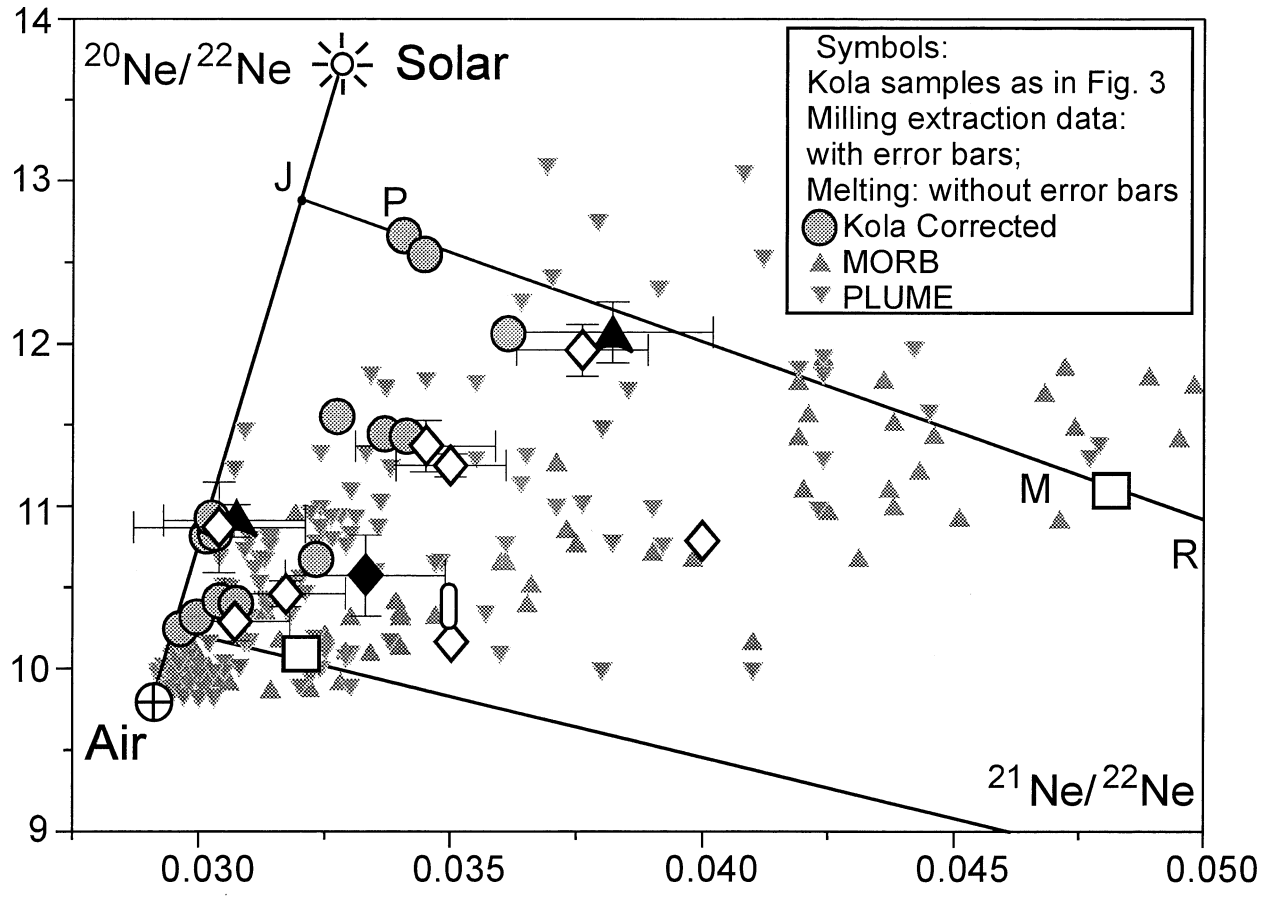

Fig. 6. Conventional Ne three-isotope plot indicates mixing between atmospheric (Air), primordial (Solar) and radiogenic end-members. The isotopic ratios in Ne extracted by crushing (Marty et al., 1998, data-points shown with error bars) follow the plume-like trend situated slightly to the right off Loihi plume array, whereas the whole-rock ratios (Tolstikhin et al., 1985) approach the MORB array. When in-situ produced ^{21}Ne* and ^{22}Ne* were subtracted from the measured whole-rock abundances using He-Ne systematic (see text), the resulting data-points shift to the left-top and joint the plume trend. See Figure 3 for symbols and sources of MORB and PLUME data.

fluid-bearing minerals, e.g., phlogopite and amphiboles replacing primary clynopyroxenes and olivines, also reveal this feature of Kola UACC (Veksler et al., 1998; Verhulst et al., 2000).

Step-wise heating experiments reveal three temperature intervals, which differ by the amounts and compositions of helium liberated from Ti-magnetite and olivine (Fig. 8).

Table 3. Neon isotopes in vesicles (extracted by crushing) and bulk samples (*fusion).

Sample	Rock/mineral	^{22}Ne 10^{-12} cc/g	^{20}Ne/^{22}Ne	^{21}Ne/^{22}Ne
SB-13	Clinopyroxenite	46.7	10.57	0.0333
SB-15	Phoscorite	31.2	11.96	0.0376
SB-15	Phoscorite	36.6	11.25	0.035
SB-17	Phoscorite	8.8	11.37	0.0345
SB-17	Phoscorite	12.0	10.46	0.0317
SB-37	Carbonatite	35.1	10.29	0.0307
SB-37	Carbonatite	62.9	10.87	0.0304
LV-2	Dunite	7.6	12.07	0.0382
LV-2	Dunite	4.5	10.91	0.0307
KV-23	Phoscorite*	435.6	10.1	0.032
KV-28	Carbonatite*	245.5	11	0.048
SB-32	Carbonatite*	236.5	10.15	0.035
SB-34	Dolomite*	370.4	10.8	0.04
OV-15	Carbonatite*	288.5	10.4	0.035

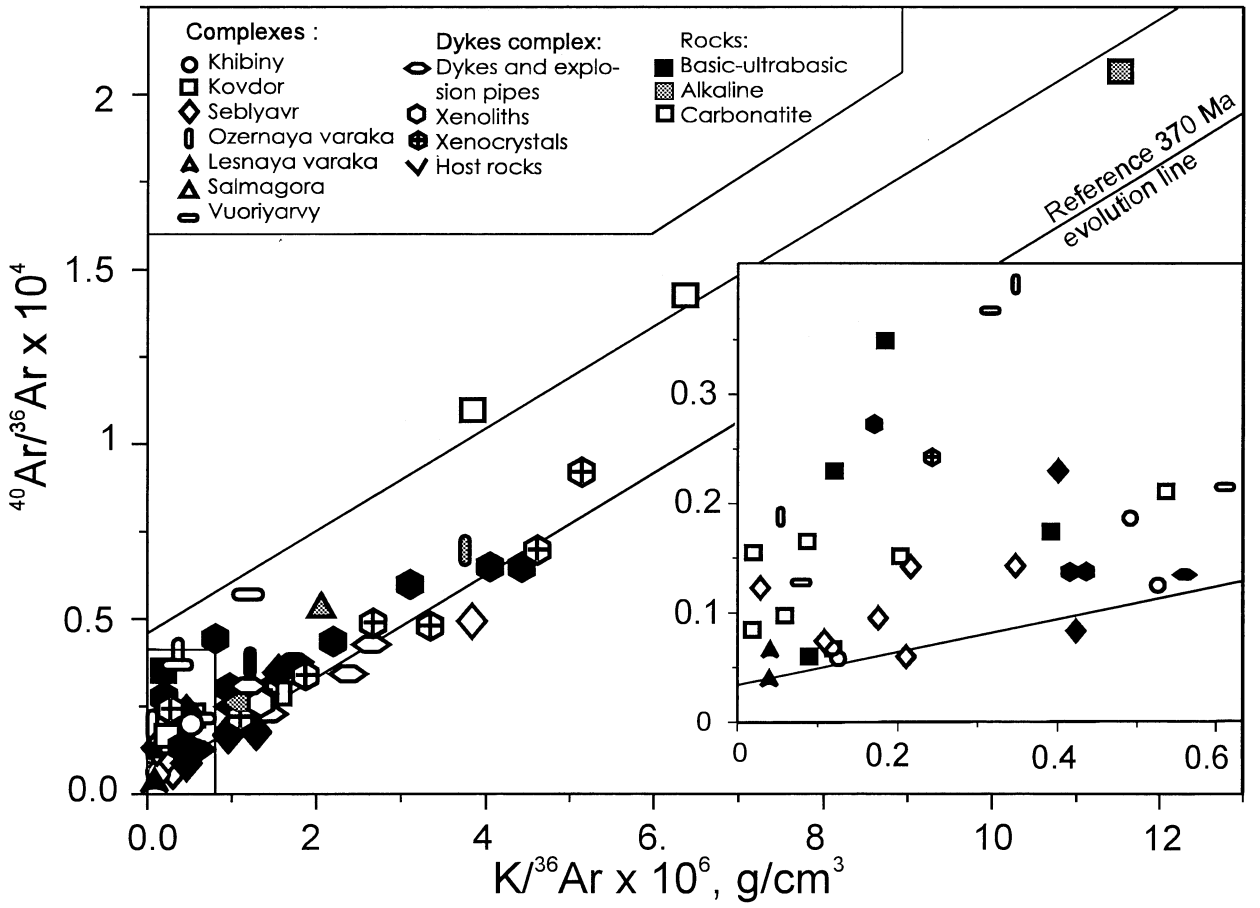

Fig. 7. K-Ar evolution diagram. Argon was extracted by fusion. Most samples approach the reference 370 Ma evolution line crossing atmospheric $^{40}Ar/^{36}Ar$ ratio. However several samples from the Kovdor (KV) and Vuoriyarvi (VR) complexes are well above the evolution line implying trapped Ar with initial $^{40}Ar/^{36}Ar \sim 4000$. Several samples having low $K/^{36}Ar$ ratios (inset) also show occurrence of excess trapped Ar with $^{40}Ar/^{36}Ar \geq 3000$. Host rocks from the dyke complex are not considered because of their older age.

1. Decrepitation of fluid inclusions at low temperatures below 800°C liberates a small portion of $^4He^*$ and ^3He.
2. Radiogenic $^4He^*$ is mainly released within a temperature interval from 600 to 1100°C. Radiation damage tracks were original sites for He*. Comparison of $^4He/^3He$ ratios in helium extracted under 800°C from Ti-magnetite BEG-1 (Fig. 8), 2.8×10^6, with that extracted under 1400°C, 9.8×10^4, implies that $^4He^*$ has been mixed with the trapped ^3He-bearing fluid only to a minor extent. Annealing of radiation tracks, most probable sites for radiogenic He*, under the moderate temperatures appears to be the main mechanism for $^4He^*$ loss.
3. In contrast to $^4He^*$, trapped ^3He is dominantly released under rather high temperatures, >1100°C, approaching melting temperatures. Step-wise heating of powder from already crushed Ti-magnetite and olivine shows a substantial, by a factor of 2, decrease of the amplitude of high-temperature ^3He peak seen in Figure 8. Definitely crushing readily liberates trapped He even though a lot of heat is required to activate its loss, whereas $^4He^*$ survives crushing. Small primary fluid inclusions appear to be appropriate sites for ^3He; decrepitation or annealing of these inclusions under high temperatures could ensure loss of the trapped fluid.

More work is needed to understand and quantify observations discussed above. Nevertheless the step-wise-heating experiments demonstrate that magnetites are promising samplers of natural fluids, including trapped mantle rare gases.

5.2. Warehouses of Mantle Fluid: Rocks and Complexes

Helium isotope abundances in different Complexes show three general tendencies (Fig. 9). (i) The $^4He/^3He$ ratios tend to increase from basic through alkaline to carbonatitic rocks. (ii) These ratios are highly variable in carbonatites. (iii) Enhanced $^4He/^3He$ ratios are typical of samples from the Ozernaya Varaka (OV), Khibiny (KH), and Dyke complexes (DC). An inverse correlation between $^4He/^3He$ ratios (bottom plot in Fig. 9) and ^3He (top), indicates that these tendencies originate mainly from variations in the ^3He concentration, which depends on processes operating at different time: (1) early processes contemporary to the magma emplacement and crystal-

Table 4. Helium and argon isotopes in mineral separates from sample SB-3.

Mineral	Size mm	^{4}He 10^{-6} cc/g	^{3}He 10^{-9} cc/g	^{4}He/^{3}He 10^6
Olivine I	>0.2	12.6	0.087	0.144
Olivine I	>0.315	8.9	0.141	0.0628
Olivine II	>0.16	50	0.135	0.369
Olivine II	>0.2	7.8	0.088	0.0885
Olivine II	>0.315	38.4	0.246	0.155
Olivine II	>0.4	54.2	0.165	0.327
Ol average		28.6	0.143	0.191
Clinopyroxene	>0.315	186.5	0.207	0.901
Clinopyroxene	>0.16	375	0.167	2.24
Cpx average		280.5	0.187	1.57
Ti-magnetite	>0.16 (3A)	338	2.74	0.123
	>0.20 (3A)	340	2.48	0.136
	>0.315 (3A)	250	2.38	0.104
	>0.315 (6A)	426	2.41	0.176
Ti-Mg average		338	2.50	0.134

The whole-rock sample has lost less than 0.5 of the radiogenic in-situ produced ^{4}He, therefore the present-day concentrations of less movable ^{3}He at least in Ol and Ti-Mgt should be similar to the initial values. A means current (amperes) used to select Ti-Mgt fractions.

lization, e.g., melt degassing and trapping of rare gases by growing minerals; (2) subsequent postmagmatic processes, e.g., production of radiogenic He* along with He migration through crystals and loss, operating during the 370 Ma long evolution of Kola UACC.

The growth of $(^4He/^3He)_{CRUSH}$ together with $(U+0.24Th)/^3He_{CRUSH}$, resulting from ^{4}He* migration and incorporation in sites where trapped He resides, indicates an important role of the postmagmatic processes (Tolstikhin et al., 1999a, 1999b).

Another way to distinguish between magmatic and postmagmatic processes is to estimate the initial concentrations of trapped helium, $^3He_{INI}$, and to compare these estimates with the observed present-day concentrations. The estimates involve assumption on similar ^{3}He and ^{4}He* loss during 370 Ma long evolution of the complexes. These two species show a different behaviour during crushing and step-wise heating extractions. Crushing readily releases a considerable fraction of trapped ^{3}He, whereas heating enables ^{4}He* to be released under temperatures lower than those liberating ^{3}He (see Fig. 8). In natural environments, the two mechanisms could have operated, supporting the above assumption. Form previous studies somewhat better retention of trapped species emerges (Mamyrin and Tolstikhin, 1984), in which case the estimated $^3He_{INI}$ represents the upper limit of the initial concentration.

The equation for radiogenic ^{4}He* generation and loss is (e.g., Bernatowicz and Podosek, 1978)

$$d^4He^*/dt = \lambda\,\gamma\,N\,(U, Th)_0 \exp(-\lambda\,T) - \theta^4He^* \qquad (2)$$

Integration and substitution of known parameters (the initial U and Th contents in a rock/mineral, the decay constant λ, the yield γ, and the age T) give the transport parameter θ, which determines the initial $^3He_{INI}$

$$^3He_{INI} \le {}^3He_{MEAS} \exp(\theta\,t). \qquad (3)$$

Figure 9 (top) includes the calculated initial concentrations, $^3He_{INI}$, which scatter mainly within a narrow range of $(4 \pm 2) \times 10^{-9}$ cm^3 g^{-1} overlapping the highest measured concentrations. Differences between the calculated initial contents and the presently observed ones emphasize the importance of postcrystallisation loss for both radiogenic and trapped He.

The Ozernaya Varaka (OV) presents an exception: the $^3He_{INI}$ concentration is well below those calculated for other complexes (Fig. 9). This implies a substantial magma degassing during formation of this complex. In agreement with this inference, intense degassing of this complex is independently suggested by the occurrence of a thick zone of fenites and fenitized gneisses (Le Bas, 1989; Ikorsky et al., 1998). The area of exposed fenitized rocks exceeds the area of magmatic (mainly alkaline) rocks by a factor of 1.6, which is ~10 times greater than for the Seblyavr (<0.2) and for the Lesnaya Varaka (0.15).

Gas loss from parent magmas and subsequently crystallised rocks is controlled, among other factors, by conditions of crystallisation including the depths of the magma chambers. Generally the less the depth, the more intense the magma degassing. However, even if mantle fluids were appreciably preserved in a chamber and trapped by crystallizing minerals, fast cooling of a shallow magma chamber would stimulate growth of imperfect crystals containing impurities, micro-fissures, vesicles, inclusions of glassy material, etc., which would cause helium loss during postcrystallisation evolution.

These conditions could be partially restored using geological and petrographical data: position of intrusions within the cross section of supracrustal rocks, quenching phases near contacts and eruptive breccias in internal parts, fingerprints of explosive processes, structural and textural peculiarities of rocks especially in contact zones. Such analysis implies that the Khiniy alkaline massif (KH) and the Dykes complex (DC) belong to the uppermost subsurface formations (Galakhov, 1975; Polkanov and U Li, 1961). The dykes are considered as eruptive channels of volcanic explosion fields removed by erosion (Bulakh and Ivanikov, 1984). These presumably low depths are in full agreement with the low ^{3}He abundances and the high ^{4}He/^{3}He ratios that indicate pre and postcrystallisation degassing (Fig. 9).

The Kovdor (KV), the Seblyavr (SB), the Vuoriyarvy (VR), and the Lesnaya Varaka (LV), showing signatures of meso-

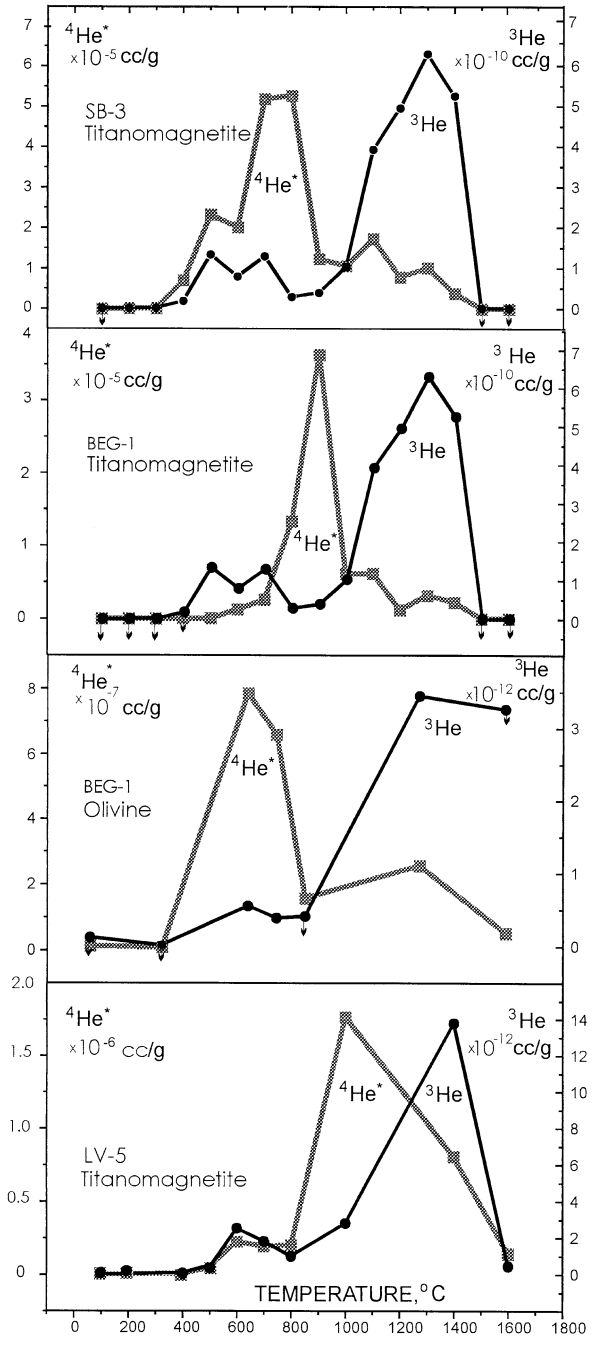

Fig. 8. Step-wise heating experiments for magnetites and olivine separated from ultrabasic rocks (see Tables 1 and 2 for SB-3 and KV-5). Arrows indicate that the upper limits of ^{3}He concentrations are shown. Notice three separated loss intervals (see text for discussion).

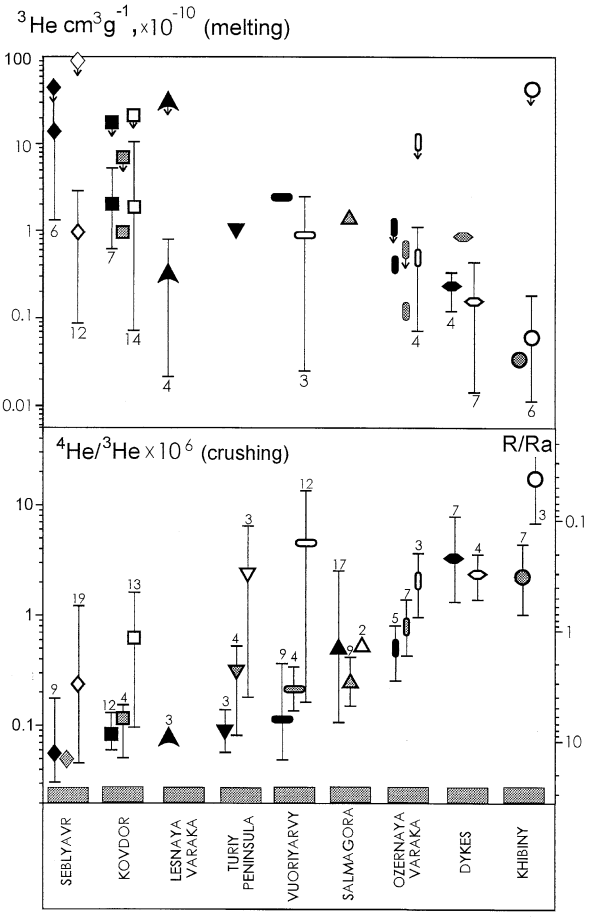

Fig. 9. ^{3}He whole rock concentrations and ^{4}He/^{3}He ratios in trapped fluid for different rocks and complexes. The Complexes are arranged in order of increasing of the average ^{4}He/^{3}He ratios in ultramafic rocks. Symbols are the average values, solid —ultrabasic, shadowed —alkaline, open —carbonatitic rocks, and bars show the limits. Symbols having arrows show the calculated initial concentrations (see text). Numbers are numbers of samples. Mirrored arrays of ^{3}He and ^{4}He/^{3}He imply trapped helium concentrations mainly govern the ^{4}He/^{3}He rations.

abyssal intrusions, were formed at greater depths (Kukharenko et al., 1965). Mineral-fluid inclusions in early apatites (the Kovdor) recorded a fluid pressure of 1.1 to 1.5 kbar corresponding to 3.5 to 5 km depth (Sokolov, 1981). The larger depths are consistent with the high ^{3}He abundances observed in rocks from these complexes. Using geological observations, Kukharenko et al. (1965) suggested intermediate depths for other complexes, again in agreement with He isotope data, except the Tury Peninsula (TP) belonging to the least degassed group (Fig. 9).

Several circumstances could ensure an exceptionally great range of rare gas concentrations in carbonatites. Carbonatitic melts are ionic liquids described by phase diagrams for silicate-carbonate-H_2O model systems (Wyllie et al., 1990). CO_2 and H_2O are volatile components of the melts, which also carry high amounts of trace volatile elements: F, Cl, P, S, and rare gases (Gittins, 1989; Woolley and Kempe, 1989; Sasada et al., 1997). This is in agreement with the high initial concentrations for Khibiny and especially Kovdor carbonatites (Fig. 9). Multiphase intrusions are typical of carbonatite magmatism, and each phase could stimulate degassing of previously formed rocks, causing variable concentrations. Carbonatites release radiogenic He easier than silicate rocks: data-points related to carbonatites constitute the bottom margin in Figure 5. This could be the case for trapped helium also: step-wise-heating

experiments indicate major loss of ^{3}He under low temperature ~500°C, in contrast to silicate minerals (Fig. 8). Therefore postmagmatic loss of He could substantially decrease the initial concentrations thus increasing the observed concentration range in carbonatites.

5.3. Primordial and Radiogenic He and Ne in Kola UACC, MORB and OIB

The radiogenic ^{4}He*/^{21}Ne* production ratio is known to be almost constant and independent of natural environments, e.g., U-bearing minerals or rocks of various composition (Kyser and Rison, 1982; Verkhovsky and Shukolukov, 1991). The latter authors reported ^{4}He*/^{21}Ne* $\approx (1.5 \pm 0.5) \times 10^7$, and Yatsevich and Honda (1997) suggested a similar value, $(2.2 \pm 0.1) \times 10^7$. A comparison of this canonical ratio with those observed in terrestrial rocks and fluids allows to study the rate of noble gas elemental fractionation and sheds light on related processes (Verkhovsky et al., 1983); this approach is used to estimate primordial ^{3}He/^{22}Ne$_{PRIM}$ ratio of the Kola plume source.

^{3}He/^{22}Ne$_{PRIM}$ versus ^{4}He*/^{21}Ne* diagram (Fig. 10) comprises Kola UACC samples along with MORB and PLUME data; all ^{3}He measured in the samples is considered as the primordial component, ^{3}He$_{MEAS} \equiv {}^3$He$_{PRIM}$, and ^{22}Ne$_{PRIM}$, ^{4}He* and ^{21}Ne* are calculated from equations:

$$^{22}\mathrm{Ne}_{\mathrm{PRIM}} = {}^{22}\mathrm{Ne}_{\mathrm{M}}\,(^{20}\mathrm{Ne}/^{22}\mathrm{Ne}_{\mathrm{M}} - {}^{20}\mathrm{Ne}/^{22}\mathrm{Ne}_{\mathrm{ATM}})/(^{20}\mathrm{Ne}/^{22}\mathrm{Ne}_{\mathrm{PRIM}} - {}^{20}\mathrm{Ne}/^{22}\mathrm{Ne}_{\mathrm{ATM}}) \quad (4)$$

$$^4\mathrm{He}^* = {}^3\mathrm{He}_{\mathrm{M}}\,(^4\mathrm{He}/^3\mathrm{He}_{\mathrm{M}} - {}^4\mathrm{He}/^3\mathrm{He}_{\mathrm{PRIM}}) \quad (5)$$

$$^{21}\mathrm{Ne}/^{22}\mathrm{Ne}_{\mathrm{PA}} = {}^{21}\mathrm{Ne}/^{22}\mathrm{Ne}_{\mathrm{ATM}} + (^{21}\mathrm{Ne}/^{22}\mathrm{Ne}_{\mathrm{PRIM}} - {}^{21}\mathrm{Ne}/^{22}\mathrm{Ne}_{\mathrm{ATM}})\,[(^{20}\mathrm{Ne}/^{22}\mathrm{Ne}_{\mathrm{M}} - {}^{20}\mathrm{Ne}/^{22}\mathrm{Ne}_{\mathrm{ATM}})/(^{20}\mathrm{Ne}/^{22}\mathrm{Ne}_{\mathrm{PRIM}} - {}^{20}\mathrm{Ne}/^{22}\mathrm{Ne}_{\mathrm{ATM}})] \quad (6)$$

$$^{21}\mathrm{Ne}^* = {}^{22}\mathrm{Ne}_{\mathrm{M}}\,(^{21}\mathrm{Ne}/^{22}\mathrm{Ne}_{\mathrm{M}} - {}^{21}\mathrm{Ne}/^{22}\mathrm{Ne}_{\mathrm{PA}}), \quad (7)$$

where subscripts M, ATM define measured and atmospheric values, respectively; the proportion of mixing of solar (see Section 4.3) and atmospheric species in each individual sample gives the PA values.

The measured ratios of both radiogenic and primordial species vary within 4 orders of magnitude and correlate, as it was shown independently by Honda (1998) and Tolstikhin et al. (1998). All but one Kola samples are within the MORB-PLUME array, deviating from the canonical ratios towards both higher and lower values.

The primordial rare gases, e.g., ^{3}He and ^{22}Ne$_{PRIM}$, could not survive in a severely degassed upper mantle since the Earth accretion 4.5 Ga ago (e.g., Tolstikhin and Marty, 1998). Therefore they should be derived from a deep plume source, which supplies the upper mantle with primordial rare gases. The mean residence time of these species, as well as other highly incompatible elements in the upper mantle is ~1 Ga (Galer and O'Nions, 1985). During this time interval the isotopic compositions were biased towards more radiogenic MORB ones due to contribution of ^{4}He* and ^{21}Ne* generated in mantle rocks (O'Nions and Oxburgh, 1983; Kellogg and Wasserburg, 1990; O'Nions and Tolstikhin, 1994, 1996; Porcelli and Wasserburg, 1995).

A fractionation event responsible for the direct correlation, which is identical for both MORB and PLUME samples (Fig. 10), could only have occurred after sizeable production of radiogenic isotopes, i.e., slightly before, during or after the melt intrusion into the crust. Otherwise the ratios between ancient primordial (^{3}He, ^{22}Ne$_{PRIM}$) and newly produced radiogenic (^{4}He* and ^{21}Ne*) species were not correlated.

Transferring the mean ^{4}He*/^{21}Ne* production ratio, $(1.5 \pm 0.5) \times 10^7$, via the regression line to the ^{3}He/^{22}Ne$_{PRIM}$ axis allows the prefractionation ^{3}He/^{22}Ne$_{PRIM}$ ratio to be recovered, ^{3}He/^{22}Ne$_{PRIM} \approx 10$, similar to 7.7 derived by Honda and Patterson (1999). Both values are comparable with the post-D-burning solar ^{3}He/^{22}Ne$_{PRIM} \approx 5.3$ (^{4}He/^{20}Ne = 850 from Anders and Grevesse, 1989, and ^{4}He/^{3}He = 2200 from Geiss, 1993). This similarity suggests occurrence of the non-fractionated solar-like rare gas component deep in the mantle, in agreement with previously observed He-Ne isotopic correlations (Honda et al., 1993; Moreira and Allegre, 1998) and modelling (O'Nions and Tolstikhin, 1994; Porcelli and Wasserburg, 1995; Tolstikhin and Marty, 1998). It also lends credence to models, which envisage implanted solar gases as the major source of rare gases in proto-terrestrial materials (Tolstikhin and Marty, 1998).

A substantial decrease of He/Ne ratios (relative to the primordial/production values) could result from preferential migration and loss of He isotopes from vehicles in basalt glasses and/or from rock + vehicles system as a whole (Mamyrin and Tolstikhin, 1984). Helium shows much higher penetrability through silicates than Ne and Ar (Aschkinadze, 1980; Morozova and Aschkinadze, 1971) and specifically through silicate glasses, which are the major noble gas hosts in ocean ridge and seamount environments.

A 50-fold increase of He/Ne ratios requires a special explanation. Tolstikhin et al. (1999a) have shown that such a trend could not originate from partial melt degassing (Spasennykh and Tolstikhin, 1993) owing to a better solubility of He in silicate melts than the solubilities of heavier gases (Jambon et al., 1986; Lux, 1987). The preferential helium loss from basalt glasses proposed above produces high He/Ne ratios in a complementary fluid phase. Helium concentrations in the fluids could be even higher than the concentrations in the fluid-bearing rocks. Then some "secondary" process could fix these high concentrations and ratios. For example the fluid could be accumulated in later formed vesicles, or later portions of melt could trap the fluid, etc. Also a non-equilibrium degassing process, when He migrates into ascending bubbles faster than Ne, could be responsible for the enhanced He/Ne ratios. More work is needed to model and quantify these processes.

5.4. Mantle Sources of Plume-Related Component

Similar isotopic and chemical characteristics of rocks, originating from small-volume continental magmas, and of alkali basalts from oceanic islands or seamounts call for common source(s) and processes. While both astenospheric (Kwon et al., 1989; Nelson et al., 1988) and lithospheric (McKenzie and O'Nions, 1995) source regions were suggested on the ground of isotopic arguments, models of generation and development of

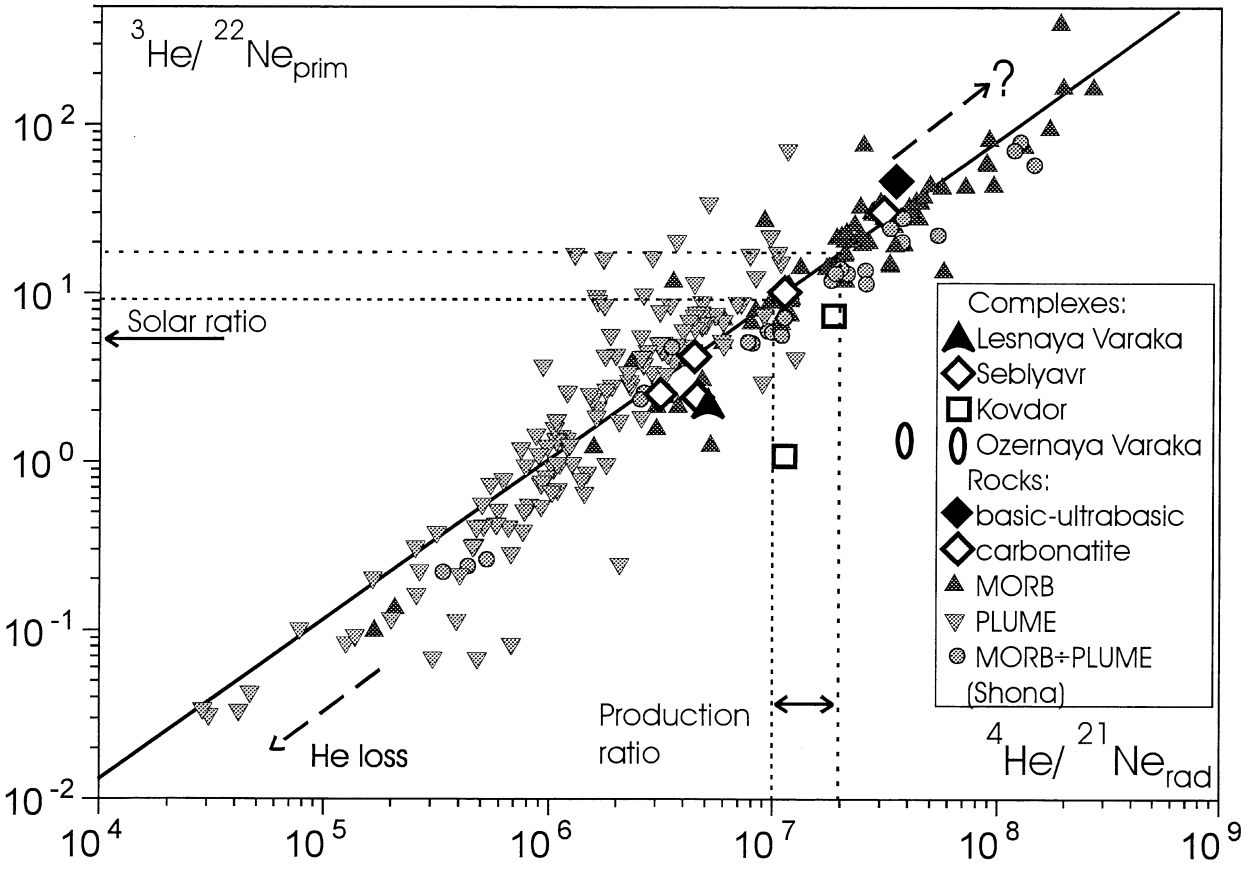

Fig. 10. Primordial and radiogenic He and Ne in samples from Kola UACC, MORB and OIB. While the $^4He^*/^{21}Ne^*$ production ratio is almost constant, both observed $^4He^*/^{21}Ne^*$ and $^3He/^{22}Ne_{PRIM}$ vary within a great range. Projection of the canonical production ratio to the regression line and further onto the Y axis indicates $^3He/^{22}Ne$ similar to the actual solar value. The latter implies solar-like relative abundances of ^3He and ^{22}Ne in the mantle before the fractionation. Possible mechanisms responsible for the fractionation of helium and neon isotopes are discussed in the text. See Figure 3 for sources of MORB and OIB data.

carbon- and alkali-rich melt generally envisage a metasomatically enriched lithospheric source (Wyllie et al., 1990). The discussion below follows a model, which incorporates isotopic, geochemical, geochronological, and geophysical data (McKenzie and O'Nions, 1995). As the most plausible environment the model envisages a two-layered subcontinental lithosphere, including a MORB-source-like bottom layer and a depleted (relative to the MORB source) top one. These layers were processed by metasomatic melts (10 to 30%) originating from extraction of ~0.3 to 0.5% melt from the astenospheric mantle. Because the subcontinetal lithosphere is a long-life conservative reservoir (Kramers, 1979; 1991; Richardson et al., 1984), the time interval between the metasomatic processing and the mobilisation of parent ultrabasic-alkaline-carbonatitic magmas could be long and variable. The long time interval allows enriched (relative to the MORB) isotopic signatures to be generated.

This time interval is crucial to constrain the ^3He-bearing source for Kola UAC complexes. It should be emphasised that both trace-element- (McKenzie and O'Nions, 1995) and major-element-related (Wyllie et al., 1990) models do not consider a plume source for metasomatic melts. In the past, the upper astenospheric mantle could also show lower $^4He/^3He$ ratios due to e.g., a higher flux of ^3He rich material from the plume source(s). To understand whether the ancient upper mantle could be a source of low-$^4He/^3He$ melts, the age, when this reservoir had a $^4He/^3He$ ratio similar to that in the UACC parent melts, should be compared with the age of metasomatism inferring from more reliable isotopic systematics, e.g., Rb-Sr or Sm-Nd.

Inspection of rare gas evolutionary degassing models (Azbel and Tolstikhin, 1990; Tolstikhin and Marty, 1998) shows that $^4He/^3He_{DM}$ ratios in the astenospheric depleted mantle, source of MORB, could be similar to or lower than the Kola UACC initial value ~3 Ga ago or earlier. The model post 3-Ga $^4He/^3He_{DM}$ ratios always exceed the initial Kola value (see Fig. 5). Therefore the astenospheric upper mantle could have been a source of the metasomatic melts ~3 Ga ago.

In contrast to the above quite ancient age, a much shorter metasomatism-extraction interval is inferred from Rb-Sr systematics. The initial $^{87}Sr/^{86}Sr$ ratios of UAC complexes, 0.7030–0.7040, are constrained by Rb-Sr isochrone dating (Kramm et al., 1993; Kramm and Kogarko, 1994) and by measuring of Sr isotope compositions in low Rb/Sr rocks/

Table 5. Contribution of principal terrestrial reservoirs to plume source

Reservoir	Contrib. (weight %)	^{22}Ne 10^{-14} mole/g	$^{20}Ne/^{22}Ne$	$^{21}Ne/^{22}Ne$	$^{4}He/^{3}He \times 10^{6}$	$^{40}Ar/^{36}Ar$	$^{3}He/^{22}Ne$	$^{36}Ar/^{22}Ne$
Lower mantle	1.8	6.05	13.7	0.0336	0.0055	5300	5.6	1.82
Upper mantle	98.2	0.07	13.7	0.0596	0.09	40000	5.56	5.34
ASW	0.06	95	9.8	0.0289	100	296	~0	80
Plume calculated	100	–	12.7	0.04	0.036	3200	4.23	21.1
Plume observed	–	–	12.6	0.04	0.03	3400	6.8	<38

Lower mantle means position of a plume source below 670 km discontinuity; because of a very small total mass flux from the source (O'Nions and Tolstikhin, 1994) its mass could be much smaller than the lower mantle mass.

ASW means air saturated water.

minerals, such as apatites or carbonatites (Dudkin et al., 1984). These ratios notaciably exceed the present day average MORB ratio 0.702 to 0.703 (Ito et al., 1987) and the lower ratios were typical of ancient mantle. The average Rb/Sr of highly differentiated UAC complexes appears to be less well constrained. Two ratios, 0.377 and 0.015, were suggested for the Lovozero and Khibiny massifs, respectively (Gerasimovsky et al., 1966; see also Kramm et al., 1993; Kukharenko and Il'insky, 1984). Substitution of the relevant ratios in equation

$$T = (1/\lambda)\ln(\{[(^{87}Sr/^{86}Sr)_{INI} - (^{87}Sr/^{86}Sr)_{DM}]/(^{87}Rb/^{86}Sr)_{INI}\} - 1) \quad (8)$$

gives a model age for upper mantle metasomatism within $T \approx$ 450 to 750 Ma ago, providing that $(^{87}Sr/^{86}Sr)_{DM}$ ratios were linearly decreasing with age (e.g., DePaolo, 1988; Azbel and Tolstikhin, 1988). Another assumption involved in the above estimate is that metasomatic processes generated the enhanced $^{87}Sr/^{86}Sr$ ratios in Kola UACC. However such ratios, ~0.703 to 0.704, are typical of ocean island basalts, which generation does not require the preeruption metasomatism. If the Kola UACC initial $^{87}Sr/^{86}Sr$ ratios were inherited from a parent melt source, then the age of respective metasomatic event could have been younger, and the above estimates should be treated as the upper limits.

The difference between U-He and Rb-Sr estimates for the age of relevant mantle fractionation processes rules out the asthenospheric depleted mantle as a source of He-bearing material and suggests that plume material, originated from a region different from the MORB mantle, supplied parent Kola UACC melts with primordial rare gases.

It is interesting to note that, following a plate-tectonic reconstruction (Torsvik et al., 1996), 450 Ma ago the Kola Peninsula (as a part of the Baltica continent) drifted approximately above the present-day position of the Ethiopian plume. This suggests that the Kola and the Ethiopian plumes could have been derived from the same deep-seated source. The low $^{4}He/^{3}He$ ratios in Oligocene flood basalts from Ethiopia, 37000 (Marty et al., 1996), are similar to the mean initial value obtained for the Kola samples, 30000 (see Fig. 5). This supports the above suggestion. It appears that the plume source stayed at about the same location on a time scale exceeding 400 Ma. The implications of such a longevity of a ^{3}He-bearing plume source relative to the life-spans of plumes themselves (e.g., the Hawaiian hot spot, the North Atlantic Volcanic Province, or the Deccan-Réunion hot spot) are of great interest for mantle dynamics.

Available model estimates of noble gas abundances in the principal terrestrial reservoirs (Tolstikhin and Marty, 1998) allow contribution of the three reservoirs, the plume source, the upper mantle, and the crust (represented by a groundwater containing presumably atmospheric gases) to be quantified (Table 5). A minor contribution from the plume implies that it could only stimulate metasomatism of the subcontinental lithosphere whereas melts from the upper mantle play the major role, in accordance with recent geochemical and petrological models (Wyllie et al., 1990; McKenzie and O'Nions, 1995) as well as with He-Sr systematics (Marty et al., 1996; Marty end Tolstikhin, 1998).

6. CONCLUDING REMARKS

1. Kola Devonian (370 Ma old) ultrabasic-alkaline-carbonatitic rocks show highly variable abundances of light rare gas isotopes. Thus, $^{4}He/^{3}He$ whole-rock ratios vary from high values expected from radiogenic production $\sim 1 \times 10^{8}$ down to 6.4×10^{4}, which is slightly below the mean MORB value, 8.6×10^{4}. While measured ^{4}He concentrations are mainly within those predicted from U and Th decays, the content of ^{3}He is up to 5×10^{-9} cc STP/g, exceeding nucleogenic in-situ production by a factor of $\sim 10^{5}$. Because of most samples were collected from boreholes or quarries, contribution of spallogenic helium is ruled out, and these concentrations (among the highest measured in terrestrial samples) together with the low $^{4}He/^{3}He$ ratios indicate the occurrence of trapped mantle fluid.
2. The isotopic compositions of fluid-related He and Ne (extracted from vesicles by crushing) definitely show a contribution of plume-related Loihi-like component. The lowest $^{4}He/^{3}He$ ratios in Kola UAC rocks, down to 3×10^{4}, are well below the MORB ratio, and in a conventional Ne isotope diagram the mantle-atmosphere mixing array for the Kola samples is indistinguishable from the Loihi array and clearly different from the MORB one.
3. Generally the spread of $^{4}He/^{3}He$ ratios in KUAC samples is decreasing with increase of ^{3}He concentrations; however even samples having quite high ^{3}He amounts show considerable, by a factor of ~50, variations of their isotopic ratios. A conventional $^{4}He/^{3}He$ versus (U+0.24Th) evolution diagram indicates a best fit initial $^{4}He/^{3}He$ ratio of 30000, the same as the lowest ratio measured in Kola UAC samples.

The estimated initial concentrations of trapped rare gases appear to be quite high and vary within a narrow range. The large $^4He/^3He$ and [^3He] variations presently observed in the samples are dominantly due to postcrystallisation production of radiogenic He and loss of trapped and radiogenic He from the samples.

4. $^{20}Ne/^{22}Ne$ versus $^{40}Ar/^{36}Ar$ correlation and K-Ar systematic give the initial $^{40}Ar/^{36}Ar \approx 4000$ to 6000 for the mantle end-member; this is about one order of magnitude lower than the value accepted for the upper mantle, source of MORB.
5. Stepwise heating experiments reveal different sites of trapped and radiogenic He isotopes. Radiogenic $^4He^*$ releases the host olivines and titanomagnetites within temperature range of 500°C to 1200°C, probably corresponding to activation of $^4He^*$-bearing radiation damage tracks. In contrast, ^3He leaves the minerals at higher temperatures of 1200°C to 1600°C, which are likely to impel annealing of $\sim 10\ \mu$ size fluid inclusions.
6. The depth of emplacement of UACC as well as the temperature regime in magma chambers controlled both melt degassing rate and ability of crystallised minerals to retain rare gases. Both characteristics govern the present-day observed abundances of rare gas isotopes. The relative emplacement depths restored from trapped/radiogenic rare gas abundances are in a good agreement with independent geological considerations.
7. Available data allow consideration of the following sequence of processes settled the Kola Devonian UAC complexes. (a) Ascent of plume material from the deep plume source to the subcontinental lithosphere; the plume triggered mantle metasomatism. (b) Metasomatism of the subcontinental lithosphere followed by magma generation and ascent, multistage intrusions, fractionation and degassing of parental melts, and fractional crystallisation ~370 Ma ago. (c) Postcrystallisation migration of fluids, including loss of radiogenic and of trapped rare gases.
8. Based on model compositions of the principle terrestrial reservoirs, the proposed contributions (by mass) of rare gas rich plume material and the upper mantle material, are 2 and 98%, respectively. A small (~0.05%) addition of air-saturated ground waters supplied atmospheric rare gases either into the parent magmas, or in already crystallised rocks/minerals.

Acknowledgments—This contribution was supported by INTAS grant 94 to 2621 and by Project 3461 from Russian Academy of Sciences. Scientific collaboration of the authors from CRPG-CNRS-Nancy and from Geological Institute, KSC RAN, was supported by grants from the French Ministry of Higher Education, from Institut National Polytechnique de Lorraine, and from International CNRS Project CNRS "Investigation of long-life mantle plumes." All authors greatly thank Rita Vetrina for help in preparing of the manuscript and John Ludden for publication of related preprint. The authors appreciated constructive comments by Dr. M. Honda, two anonymous Referees, and Prof. J. Kramers. I. Tolstikhin thanks International Space Science Institute at Bern, where he had an opportunity to work on this contribution.

Associate editor: D. E. Fisher

REFERENCES

Amelin Y. V. and Zaitsev A. (1997) A precize U-Th-Pb chronology of carbonatites and phoscorites: problems related to extreme elemental fractionation, and possible solution using multi-mineral approach. GAC/MAC Ann. Meeting. Ottawa. May. 19–21. (abstr.) Vol.P. A-2.

Anders E. and Grevesse N. (1989) Abundances of the elements: Meteoritic and solar. *Geochim. Cosmochim. Acta.* **53,** 197–214.

Andersen T. (1987) Mantle and crustal components in a carbonatite complex, and the evolution of carbonatite magma: REE and isotopic evidence from the Fen complex, southeast Norway. *Chem Geol. (Isot. Geosci. Sec)* **65,** 147–166.

Aschkinadze G. S. (1980) Migration of radiogenic isotopes in minerals. Nauka, Leningrad.

Azbel I. Y. and Tolstikhin I. N. (1988) Radiogenic isotopes and the evolution of the earth's mantle, crust and atmosphere. Kola Sci. Center Pub., Apatity.

Azbel I. Y. and Tolstikhin I. N. (1990) Geodynamics, magmatism, and degassing of the Earth. *Geochim. Cosmochim. Acta* **54,** 139–154.

Balagansky V. V., Glaznev V. N., and Osipenko L. G. (1998) Early proterozoic evolution of the Northeastern Baltic Shield: a terrain analysis. *Geotectonics* **32,** 81–92.

Bayanova T. B., Kirnarsky Y. M., and Levkovich N. V. (1997) U-Pb study of baddeleyite from the Kovdor massif. *Dokl. RAS* **356,** 509–511.

Beard A. D., Downes H., Vetrin V., Kempton P. D., and Maluski H. (1996) Petrogenesis of Devonian lamprophyre and carbonatite minor intrusions, Kandalaksha Gulf (Kola Peninsula, Russia). *Lithos* **39,** 93–119.

Beard A. D., Downes H., Hegner E., Sablukov S. M., Vetrin V. R., and Balogh K. (1998) Mineralogy and geochemistry of Devonian ultramafic minor intrusions of the southern Kola Peninsula, Russia: implications for the petrogenesis of kimberlites and melilitites. *Contrib. Mineral. Petrol.* **130,** 288–303.

Bell K. and Blenkinsop J. (1989) Neodymium and strontium isotope geochemistry of carbonatites. In *Carbonatites: Genesis and Evolution* (ed. K. Bell) pp. 360–387. Unwin Hymon: Genesis and Evolution, London.

Bernatowicz T. J. and Podosek F. A. (1978) Nuclear components in the atmosphere. In *Terrestrial Rare Gases. Advances in Earth and Planetary Sciences* (eds. E. C. Alexander and M. Ozima) pp. 99–135. Cent. Acad. Pub., Tokyo.

Bulakh A. T. and Ivanikov V. V. (1984) Problems of mineralogy and petrology of carbonatites. Leningr. St. Univ., Leningrad.

Dauphas N. and Marty B. (1999) Nitrogen and argon isotopes in carbonatites from the Kola Peninsula (Russia), an open window on the deep mantle. *Science* **286(1),** 2488–2490.

DePaolo D. J. (1988) Neodymium isotope geochemistry. Springer-Verlag. 187.

Dixon E. T., Honda M., McDougall I., Campbell I. H., and Sigurdsson I. (2000). Preservation of hear-solar neon isotopic ratios in Icelandic basalts. *Earth Planet. Sci. Lett.* **180,** 309–324.

Dudkin O. B., Minakov F. V., Kravchenko M. P., Kravchenko E. V., Kulakov A. N., Polezhaeva L. I., Pripachkin V. A., Pushkarev Y. D., and Ryungenen G. I. (1984) Khibiny carbonatites. Kola Sci. Center of USSR Acad. Sci.

Galakhov A. V. (1975) Petrology of Khibina alkaline massif. Nauka, Leningrad.

Galer S. J. G. and O'Nions R. K. (1985) Residence time of thorium, uranium and lead in the mantle and implications for mantle convection. *Nature* **316,** 778–782.

Geiss J. (1993) Primirdial Abundance of Hydrgen and Helium Isotopes. In *Origin and Evolution of the elements* (eds. Prantzos N., Vangioni F. E., Casse M.) pp. 89–106. Cambridge University Press.

Gerasimovsky V. I., Volkov V. P., Kogarko L. N., Polyakov A. I., Soprikina T. V., and Balashov Y. A. (1966) The geochemistry of the Lovozero alkaline massif. Nauka, Moscow.

Gerling E. K., Tolstikhin I. N., Drubetskoy E. R., Levkovsky R. Z., Sharkov E. V., and Kozakov I. K. (1976) Helium and argon isotopes in rock-forming minerals. *Geokhimiya* **11,** 1603–1611.

Gittins J. (1989) The origin and evolution of carbonatite magmas. In *Carbonatites: Origin and Evolution* (ed. K. Bell), pp. 580–600. Unwin Hyman, London.

Gorshkov G. V., Zjabkin V. A., Ljatkovskaya N. M., and Tsvetkov O. S. (1966) Natural neutron background of atmosphere and Earth's crust. Atomizdat, Moscow.

Grunenfelder M. H., Tilton G. R., Keith B., and Blenkinsop J. (1986) Lead and strontium isotope relationships in the Oka carbonatite complex, Quebec. *Geochim. Cosmochim. Acta* **50,** 461–468.

Hawkesworth C., Kempton P. D., Rogers N. W., Ellam R. M., and van Calsteren P. W. (1990) Continental mantle lithosphere, and shallow level enrichment processes in the Earth's mantle. *Earth Planet. Sci. Lett.* **96,** 256–268.

Hiyagon H., Ozima M., Marty B., Zashu Z., and Sakai H. (1992) Noble gases in submarine glasses from mid-oceanic ridges and Loihi seamount: Constraints on the early history of the earth. *Geochim. Cosmochim. Acta* **56,** 1301–1316.

Honda M. (1998) Systematic elemental fractionation of helium, neon and argon in MORB glasses. *ICOG-9. Chinese Sci. Bull. (abstr)* **43,** 53.

Honda M. and Patterson D. B. (1999) Systematic elemental fractionation of mantle-derived helium, neon and argon in mid-oceanic ridge glasses. *Geochim. Cosmochim. Acta* **63,** 2863–2874.

Honda M., McDougall I., Patterson D. B., Doulgeris A., and Clague D. (1991) Possible solar noble gas component in Hawaiian basalts. *Nature* **349,** 149–151.

Honda M., McDougall I., Patterson D. B., Doulgeris A., and Lague D. A. (1993) Noble gases in submarine pillow basalt glasses from Loihi and Kilauea, Hawaii: A solar component in the earth. *Geochim. Cosmochim. Acta* **57,** 859–874.

Ikorsky S. V. and Kusth V. D. (1992) Nitrogen in fluid inclusions of alkaline rocks of Khibina massif and method of its chromatographic determination. *Geochimija* **7,** 962–970.

Ikorsky S. V., Kamensky I. L., and Nivin V. A. (1997) Helium isotopic variations in the Paleozoic (380–360 Ma) complexes of the Kola Alkaline Province: High $^3He/^4He$ ratios are signs of Devonian mantle plume? EUG-9, Strasbourg 56.

Ikorsky S. V., Kamensky I. L., Nivin V. A., and Mamantov V. P. (1998) Juvenile helium migration into host rocks during formation of alkaline-ultramafic central type intrusions (on an example of Ozeraya Varaka massif, Kola Peninsula). *Dokl. RAS.* **362,** 242–244.

Ito E., White W. M., and Gopel C. (1987) The O, Sr, and Pb isotope geochemistry of MORB. *Chem. Geol.* **62,** 157–176.

Jambon A., Weber H., and Braun O. (1986) Solubility of He, Ne, Ar, Kr and Xe in basalt melt in the range 1250–1600°C. Geochemical implications. *Geochim. Cosmochim. Acta* **50,** 401–408.

Kalinkin M. I., Arzamastsev A. A., and Poljakov I. V. (1993) Kimberlites and related rocks of the Kola Region. *Petrologija* **1,** 205–214.

Kaneoka I., Takaoka N., and Upton B. G. J. (1986) Noble gas systematics in basalts and a dunite nodule from Reunion and Grand Comore Islands, Indian Ocean. *Chem. Geol.* **59,** 35–42.

Kamensky I. L., Tolstikhin I. N., Sharkov I. V., and Pushkarev Y. D. (1984) The first results of measuring helium isotopic composition on single-cascade mass-spectrometer MI-1201. *Geokhimiya* **3,** 439–443.

Kellogg L. H. and Wasserburg G. J. (1990) The role of plumes in mantle helium fluxes. *Earth Planet Sci. Lett.* **99,** 276–289.

Kogarko L. N., Kononova V. A., Orlova M. P., and Wooley A. R. (1995) Alkaline Rocks and Carbonatites of the World. Part. 2, Former USSR. Chapman and Hall., London.

Kramers J. D. (1979) Lead, uranium, strontium, potassium and rubidium in inclusion-bearing diamonds and mantle derived xenoliths from Southern Africa. *Earth Planet. Sci. Lett.* **42,** 58–70.

Kramers J. R. (1991) Paradoxes of the mantle lithosphere underneath Archaean continents and models for its origin. *Schweiz. Mineral. Petrogr. Mitt.* **71,** 175–186.

Kramm U. and Kogarko L. N. (1994) Nd and Sr isotope signatures of the Khibina and Lovozero agpaitic centres, Kola Alkaline Province, Russia. *Lithos* **32,** 225–242.

Kramm U., Kogarko L. N., Kononova V. A., and Varrtianen H. (1993) The Kola Alkaline Province of the CIS and Finland: Precise Rb-Sr ages define 380–360 Ma age range for all magmatism. *Lithos* **30,** 33–44.

Kratz K. O. (1978) Earth's crust of Eastern part of the Baltic Shield. Nauka, Leningrad.

Kukharenko A. A. (1967) Alkaline magmatism in Eastern part of the Baltic Shield. *Zap. VMO* **96,** 5 547–566.

Kukharenko A. A. and Il'insky G. A. (1984) Corrected data on average concentrations of elements in rocks of the Khibiny massif. *Zap. VMO* **113,** 4, 393–397.

Kukharenko A. A., Orlova M. P., Bulakh A. G., Bagdasarov E. A., Rimskaya-Korsakova O. M., Nefedov E. I., Il'insky G. A., Sergeev A. S., and Abakumova N. B. (1965) Kaledonian complex of ultrabasic, alkaline rocks and carbonatites of Kola Peninsula. Nedra, Moscow.

Kwon S-T., Tilton G. R., and Grunenfelder M. H. (1989) Lead isotope relationships in carbonatites and alkalic complexes: An overview. In *Carbonatites: Genesis and Evolution* (ed. K. Bell) pp. 360–387. Unwin Hymon, London.

Kyser T. K. and Rison W. (1982) Systematics of rare gas isotopes in basic lavas and ultramafic xenoliths. *Geophys. Res.* **87,** 5611–5630.

Le Bas M. J. (1987) Nephelenites and carbonatites In *Alkaline Igneous Rocks* (eds. J. G. Fitton and B. G. Upton.). Geol. Soc. Special Pub. **30,** 53–83.

Le Bas M. J. (1989) Diversification of carbonatite. In *Carbonatites: genesis and evolution* (ed. K. Bell) pp. 428–446. Unwin Hymon, London.

Lux G. (1987) The behaviour of noble gases in silicate liquids: solution, diffusion, bubbles and surface effects, with implications to natural samples. *Geochim. Cosmochim. Acta* **51,** 1549–1560.

Mamyrin B. A. and Tolstikhin I. N. (1984) Helium isotopes in nature. Elsevier Sci. Pub., Amsterdam.

Marty B. (1989) Neon and xenon isotopes in MORB: implications for the earth-atmosphere evolution. *Earth Planet. Sci. Lett.* **94,** 45–56.

Marty B. and Lussiez P. (1993) Constraints on rare gas partition coefficients from analysis of olivine-glass from a picritic mid-ocean ridge basalt. *Chem. Geol.* **106,** 1–7.

Marty B. and Humbert F. (1997) Nitrogen and argon isotopes in oceanic basalt. *Earth Planet. Sci. Lett.* **152,** 101–112.

Marty B. and Tolstikhin I.N. (1998) CO_2 fluxes from mid-ocean ridges, arcs and plumes. *Chem. Geol.* **145,** 233–248.

Marty B., Pik R., and Gezahegn Y. (1996) Helium isotopic variations in Ethiopian Plume Lavas: Nature of Magmatic sources and Limit on Lower Mantle Contribution. *Earth Planet. Sci. Lett.* **144,** 223–237.

Marty B., Tolstikhin I., Kamensky I. L., Nivin V., Balaganskaya E., and Zimmermann J.-L. (1998) Plume-derived rare gases in 380 Ma carbonatites from the Kola region (Russian) and the argon isotopic composition in the deep mantle. *Earth Planet. Sci. Lett.* **164,** 179–192.

McKenzie D. and O'Nions R. K. (1995) The source regions of ocean island basalts. *J. Petrol.* **36,** 133–159.

Mitrofanov F. P., Ikorsky S. V., and Kamensky I. L. (1995) He isotopes in Paleozoic alkaline intrusives of Kola Peninsula and Northern Karelija. *Dokl. RAS* **345,** 243–246.

Moreira M., Staudacher T., Sarda P., Schilling J. G., and Allegre C. J. (1995) A primitive plume neon component in MORB: the Samoa ridge-anomaly, South Atlantic (51–52°S). *Earth Planet. Sci. Lett.* **133,** 367–377.

Moreira M. and Allegre C. J. (1998) Helium-neon systematics and the structure of the mantle. *Chem. Geol.* **147,** 53–59.

Morozova I. M. and Aschkinadze G. S. (1971) Migration of rare gas atoms in minerals. Nauka, Leningrad.

Morrison P. and Pine J. (1955) Radoigenic origin of the helium isotopes in rock. *Ann. New York Academ. Sci.* **62,** 69–92.

Nelson D. R., Chivas A. R., Chappell B. W., and McCulloch M. T. (1988) Geochemical and isotopic systematics in carbonatites and implication for the evolution of ocean-island sources. *Geochim. Cosmochim. Acta* **52,** 1–17.

O'Nions R. K., and Oxburgh E. R. (1983) Heat and helium in the Earth. *Nature* **306,** 429–432.

O'Nions R. K. and Tolstikhin I. N. (1994) Behaviour and residence times of lithophile and rare gas tracers in the upper mantle. *Earth Planet. Sci. Lett.* **124,** 131–138.

O'Nions R. K. and Tolstikhin I. N. (1996) Limits on mass flux between lower and upper mantle and stability of layering. *Earth Planet. Sci. Lett.* **139,** 213–222.

Ozima M. and Zashu S. (1983) Noble gases in submarine pillow volcanic glases. *Earth Planet. Sci. Lett.* **62,** 24–40.

Polkanov A. A. and U Li J. (1961) On genesis and evolution of alkaline magma of Khibina subvulkano. Questions of geochronology and geology. *Proc. Lab. Geol. Dokembr. USSR Acad. Sci.* **12,** 176–186.

Porcelli D. and Wasserburg G. J. (1995) Mass transfer of helium, neon, argon and xenon through a steady-state upper mantle. *Geochim. Cosmoshim. Acta* **59,** 4921–4937.

Poreda R. and di Brozolo F. R. (1984) Neon isotope variations in Mid-Atlantic Ridge basalts. *Earth Planet. Sci. Lett.* **69,** 277–289.

Poreda R. J. and Farley K. A. (1992) Rare gases in Samoan xenoliths. *Earth Planet. Sci. Lett.* **113,** 129–144.

Richard D., Marty B., and Chaussidon M. (1996) Helium isotopic evidence for a lower mantle component in depleted Archean komatiite. *Science* **273,** 93–95.

Richardson S. H., Gurney J. J., Erlank A. J., and Harris J. W. (1984) Origin of diamonds in old enriched mantle. *Nature* **310,** 198–202.

Rundkvist D. V. and Mitrofanov F. P. (1988) Precambrian geology of the USSR. Nauka, Leningrad.

Sarda P., Staudacher T., and Allegre C. J. (1985) $^{40}Ar/^{36}Ar$ in MORB glasses: constraints on atmosphere and mantle evolution. *Earth Planet. Sci. Lett.* **72,** 357–375.

Sarda P., Staudacher T., and Allegre C. J. (1988) Neon isotopes in submarine basalts. *Earth Planet. Sci. Lett.* **91,** 73–88.

Sasada T., Hiyagon H., Bell K., and Ebihara M. (1997) Mantle-derived noble gases in carbonatites. *Geochim. Cosmochim. Acta* **61,** 4219–4228.

Sokolov S. V. (1981) New data for the Kovdor apatite-magnetite deposit formation. *Zap. VMO* **110,** 5, 581–588.

Spasennykh M. Y. and Tolstikhin I. N. (1993) Noble gas fractionation during degassing of melts. *Geochim. J.* **27,** 213–217.

Staudacher T. and Allegre C. J. (1982) Terrestrial xenology. *Earth Planet. Sci. Lett.* **60,** 389–406.

Staudacher T. and Allegre C. J. (1989) Noble gases in glass samples from Tahiti: Teahitia, Rocard and Mehetia. *Earth Planet. Sci. Lett.* **93,** 210–222.

Staudacher T., Kurz M. D., and Allegre C. J. (1986) New noble-gas data on glass samples from Loihi seamount and Hualalai and on dunites samples from Loihi and Reunion Island. *Chem. Geol.* **56,** 193–205.

Staudacher T., Sarda P., Richardson S. H., Allegre C. J., Sanga I., and Dmitriev L. V. (1989) Noble gases in basalt glasses from a Mid-Atlantic ridge topographic high at 14°N: Geodynamic consequences. *Earth Planet. Sci. Lett.* **96,** 119–133.

Subbotin V. V. and Mihaelis S. A. (1986) Genetic types of apatite ores from Sebljavr complex deposit. In *Deposits of ore-free raw materials on Kola PeninsulaY* (ed. O. B. Dudkin.) pp. 27–35. Kola Sci. Center Russian Acad. Sci., Apatity.

Taylor S. R. and McLennan S. M. (1985) The continental crust: its composition and evolution. Blackwell Sci. Pub., Oxford.

Tolstikhin I. N. and Marty B. (1998) The evolution of terrestrial volatiles: A view from helium, neon, argon and nitrogen isotope modelling. *Chem. Geol.* **147,** 27–52.

Tolstikhin I. N., Kamensky I. L., Sharkov I. V., Dudkin O. B., and Pripachkin V. A. (1985) Isotopes of light inert gases in the carbonatites of Kola Peninsula. Kola Sci. Center Russian Acad. Sci., Apatity.

Tolstikhin I. N., Lehmann B. E., Loosli H. H., and Gautschi A. (1996) Helium and argon isotopes in rocks, minerals and related groundwaters: A case study in Northern Switzerland. *Geochim. Cosmochim. Acta* **60,** 1497–1514.

Tolstikhin I. N., Kamensky I. L., Ikorsky S. V., Nivin V. A., Balaganskaya E. G., Vetrin V. R., and Gannibal M. (1998) Loihi-Like plume component in Devonian Kola ultrabasic-alkaline rocks and carbonatites: noble gas evidence (abstr.). *ICOG-9. Chi. Sci. Bull.* **43,** 131.

Tolstikhin I. N., Kamensky I. L., Marty B., Nivin V. A., Vetrin V. R., Balaganskaya E. G., Ikorsky S., Gannibal M., Kirnarsky Y. M., Weiss D., Verhulst A., and Demaiffe D. (1999a) Lower mantle plume component in Devonian Kola ultrabasic-alkaline-carbonatite complexes: evidences from rare gas isotopes and related parent elements. Apatity-Nancy-Bruxelles.

Tolstikhin I. N., Kamensky I. L., Nivin V. A., Vetrin V. R., Balaganskaya E. G., Ikorsky S. V., Gannibal M. A., Kirnarsky Y. M., Marty B., Weiss D., Verhulst A., and D. D. (1999b) Low mantle plume component in 370 Ma old Kola ultrabasic-alkaline-carbonatite complexes: Evidences from rare gas isotopes and related trace elements. *Russ. J. of Earth Sci.* **1(2),** 179–222.

Torsvik T. H., Smethurst M. A., Meert J. G., VanderVoo R., McKerrow W. S., Brasier M. D., Sturt B. A., and Walderhaug H. J. (1996) Continental break-up and collision in the Neoproterozoic and Palaeozoic-A tale of Baltica and Laurentia. *Earth-Sci. Rev.* **40(3–4),** 229–258.

Valbracht P. J., Honda M., Matsumoto T., Mattielli N., McDougall I., Ragettli R., and Weis D. (1996) Helium, neon and argon isotope systematics in Kerguelen ultramafic xenoliths: implication for mantle source signatures. *Earth Planet. Sci. Lett.* **138,** 29–38.

Veksler I. V., Nielsen T. F. D., and Sokolov S. V. (1998) Mineralogy of crystallized melt inclusions from Gardiner and Kovdor ultramafic alkaline complexes: implications for carbonatite genesis. *J. Petrol.* **39,** 2015–2031.

Verkhovsky A. B. and Shukolukov Y. A. (1991) Element and Isotope Fractionation of Noble Gases in Nature. Nauka, Moscow.

Verkhovsky A:B., Yurgina E. K., and Shukolukov Y. A. (1983) Element and isotope ratios of juvenile noble gases. *Geokhimiya* **11,** 1559–1576.

Verhulst A., Balaganskaya E., Kirnarsky Y., and Demaiffe D. (2000). Petrological and geochemical (trace elements and Sr-Nd isotopes) characteristics of the Paleozoic Kovdor ultramafic, alkaline and carbonatite intrusion (Kola Peninsula, NW Russia). *Lithos* **51,** 1–25.

Vetrin V. R. and Kalinkin M. M. (1992) Reconstruction of the processes of intracrustal and crustal-mantle magmatism and metasomatism. Kola Sci. Centre Pub., Apatity.

Woolley A. R. and Kempe D. R. C. (1989) Carbonatites: nomenclature, averege chemical compositions, and element distribution. In *Carbonatites: Origin and Evolution.* (ed. K. Bell). pp. 1–13. Unwin Hymon, London

Wyllie P. J., Baker M. B., and White B. (1990) Experimental boundaries for the origin and evolution of carbonatites. *Lithos* **26,** 3–19.

Yatsevich I. and Honda M. (1997) Production of nucleogenic neon in the Earth from natural radioactive decay. *J. Geophys. Res.* **102(B5),** 10291–10298.

Zaitsev A. N. and Bell K. (1995) Sr and Nd isotope data of apatite, calcite and dolomite as indicators of source and the relationships of phoscorites and carbonatites from the Kovdor massif, Kola Peninsular, Russia. *Contrib. Miner. Petrol.* **121,** 324–335.

Zaitsev A. N., Bell K., Wall F., and Le Bas M. J. (1997) Alkaline-REE-bearing carbonates from carbonatites of Khibina massif: mineralogy and origin. *Dokl. RAS* **335,** 241–245.

Zartman R. E., Wasserburg G. J., and Reynolds J. H. (1961) Helium, argon and carbon in some natural gases. *Geophys. Res.* **66,** 1, 277–306.